Dynamics of vortex penetration, jumpwise instabilities, and nonlinear surface resistance of type-II superconductors in strong rf fields

A. Gurevich[1] and G. Ciovati[2]
[1]*National High Magnetic Field Laboratory, Florida State University, Tallahassee, Florida 32310, USA*
[2]*Thomas Jefferson National Accelerator Facility, Newport News, Virginia 23606, USA*
(Received 7 September 2007; published 4 March 2008)

We consider the nonlinear dynamics of a single vortex in a superconductor in a strong rf magnetic field $B_0 \sin \omega t$. Using the London theory, we calculate the dissipated power $Q(B_0, \omega)$ and the transient time scales of vortex motion. For the linear Bardeen-Stephen viscous drag force, vortex velocities reach unphysically high values during vortex penetration through the oscillating surface barrier. It is shown that penetration of a single vortex through the ac surface barrier always involves penetration of an antivortex and the subsequent annihilation of the vortex-antivortex pairs. Using the nonlinear Larkin-Ovchinnikov (LO) viscous drag force at higher vortex velocities $v(t)$ results in a jumpwise vortex penetration through the surface barrier and a significant increase of the dissipated power. We calculate the effect of dissipation on the nonlinear vortex viscosity $\eta(v)$ and the rf vortex dynamics and show that it can also result in the LO-type behavior, instabilities, and thermal localization of penetrating vortex channels. We propose a thermal feedback model of $\eta(v)$, which not only results in the LO dependence of $\eta(v)$ for a steady-state motion, but also takes into account retardation of the temperature field around a rapidly accelerating vortex and a long-range interaction with the surface. We also address the effect of pinning on the nonlinear rf vortex dynamics and the effect of trapped magnetic flux on the surface resistance R_s calculated as a function of rf frequency and field. It is shown that trapped flux can result in a temperature-independent residual resistance R_i at low T and a hysteretic low-field dependence of $R_i(B_0)$, which can *decrease* as B_0 is increased, reaching a minimum at B_0 much smaller than the thermodynamic critical field B_c. We propose that cycling of the rf field can reduce R_i due to rf annealing of the magnetic flux which is pumped out by the rf field from a thin surface layer of the order of the London penetration depth.

DOI: 10.1103/PhysRevB.77.104501 PACS number(s): 74.25.Nf, 74.25.Qt, 74.25.Op

I. INTRODUCTION

The behavior of superconductors in strong rf fields involves many complex mechanisms related to a nonlinear electromagnetic response of nonequilibrium quasiparticles, pair-breaking suppression of the superconducting gap Δ, and penetration of vortices at higher rf amplitudes.[1,2] The physics behind the nonlinear rf response has recently attracted much attention due to the development of a new generation of high-performance superconducting Nb cavities for particle accelerators, in which the peak surface GHz fields $B(t) = B_0 \sin \omega t$ close to the thermodynamic critical field B_c were reached at a very high quality factor $\sim 10^9 - 10^{11}$ characteristic of the Meissner state.[3,4] At such strong rf fields the peak surface current density $B_0/\mu_0\lambda$ approaches the depairing current density J_d at which the Meissner state becomes unstable with respect to avalanche penetration of vortices once the instantaneous rf field $B(t) = B_0 \sin \omega t$ exceeds the superheating field $B_s \approx B_c$. In turn, penetration of vortices causes a sharp increase in the surface resistance R_s.

As far as the very high quality factors are concerned, of particular interest is the behavior of R_s in s-wave superconductors at low temperatures $T \ll T_c$ and frequencies $\omega \ll \Delta$, for which the rf field cannot break the Cooper pairs, and the very low Meissner surface resistance $R_s \propto (\omega^2 \Delta/T)\exp(-\Delta/T)$ is due to an exponentially small density of thermally activated quasiparticles [unlike the power-law dependence $R_s(T) \simeq R_i + CT^\alpha$ due to nodal quasiparticles in d-wave superconductors[5–8]]. In this case penetration of even a few vortices driven by extremely high rf currents densities $J \sim J_d$ can produce strong energy dissipation comparable to that in the Meissner state, which, in turn, can trigger thermomagnetic flux avalanches and the superconductivity breakdown. It is therefore important to understand dynamics of single-vortex penetration under strong rf fields. Yet the rf field onset of vortex penetration B_v, the dissipated power Q as functions of B_0 and ω, and the relation between B_v and the thermodynamic B_c and the lower critical field B_{c1} are still not well understood. These problems include complex kinetics of the emergence of the vortex core at the surface and the subsequent nonlinear large-amplitude oscillation of the vortex at the surface driven by strong rf currents much higher than the depinning critical current density. This situation cannot be described by the theory of linear electrodynamics of a pinned mixed state weakly deformed by rf currents.[9–12] Some issues of vortex dynamics in ramping magnetic fields have been addressed in numerical simulations of the time-dependent Ginzburg-Landau (TDGL) equations[13–17] valid at $T \approx T_c$, molecular dynamics simulations,[18] or in the theory of macroscopic nonlinear electrodynamics of pinned mixes states.[19,20] However, few experimental and theoretical results on vortices driven by very strong rf currents at low temperatures have been published in the literature.

In this paper we address the nonlinear rf dynamics of a single vortex moving in and out of a type-II superconductor through an oscillating magnetic surface barrier locally weakened by a surface defect. We show that in this seemingly basic situation weak Meissner fields $B_0 \ll B_c$ can drive the vortex with velocities $v(t)$ so high that the linear Bardeen-Stephen viscous drag model becomes inadequate. As a result,

the vortex velocity $v(t)$ can exceed the sound velocity, causing the Cherenkov generation of hypersound.[21,22] Moreover, $v(t)$ can exceed the critical velocity v_0, above which the vortex drag coefficient $\eta(v)$ decreases as v increases, and the viscous drag force $f_v = v\,\eta(v)$ reaches maximum at the critical velocity v_0, resulting in the jumpwise Larkin-Ovchinnikov (LO) instability.[23,24] The LO instability has been extensively investigated by dc transport measurements[25–31] on both low-T_c and high-T_c superconductors for which $v_0 \simeq 1-10$ km/s have been typically observed at low T and B. Single-vortex dynamics under a strong rf field also involves annihilation of vortex-antivortex pairs and a cascade of single-, double-, and multiple-vortex penetrations. Competition of the rf driving force, image attraction to the surface, and the viscous drag force results in a strong dependence of the dissipated power Q on the rf amplitude and frequency. Very high vortex velocities achieved at fields $B_0 \sim B_c$ required to break the surface barrier make it possible to probe the behavior of vortices under extreme conditions, for which the Lorentz driving force approaches its ultimate depairing limit. Because of strong heating effects, these conditions are hard to reproduce in transport experiments (except in high-power pulse measurements[32,33]). The importance of heating effects for transport instabilities in superconductors at low temperatures is well known.[24,34–36] In this paper we show that heating is a key limiting factor for the high-field surface resistance at $T \ll T_c$ as well, even for single vortices driven by strong rf Meissner currents. In particular, viscous vortex dynamics coupled with electron overheating can result in the LO-type behavior of $\eta(v)$, thermal rf breakdown, and a long-range interaction (on scales much greater than the London penetration depth) between a vortex and the surface and between vortices themselves.

The paper is organized as follows. In Sec. II we establish the main parameters of interest by considering the penetration and dissipation of a single vortex over the oscillating surface barrier in type-II superconductors described by the dynamic equation, in which the linear Bardeen-Stephen viscous drag force is balanced by the Lorentz driving force and the image attraction force at the surface in the London theory. Even in this basic model rf vortex dynamics always involves annihilation of vortex-antivortex pairs for $B_0 \approx B_v$ close to the penetration field B_v and a strong dependence of the dissipated power $Q(B_0, \omega)$ on the rf frequency and amplitude. In Sec. III we show that the Bardeen-Stephen model actually has a very limited applicability because vortices breaking through the surface barrier reach supersonic velocity, so the velocity dependence of the viscous drag coefficient $\eta(v)$ must be taken into account. In this case the vortex dynamics becomes strongly coupled with nonequilibrium overheating of the vortex core, resulting in a jumpwise penetration of single vortices through the surface barrier and a significant increase in Q. In Sec. IV we consider the effect of pinning on the rf surface resistance. In particular, we show that trapped vortices can result in a temperature-independent, field-hysteretic residual resistance, which can *decrease* as the rf field increases. Pinned vortices can also produce hot spots, which ignite thermal rf breakdown. Section V is devoted to dissipation around hot spots and their nonlinear contribution to the global surface resistance. The thermal breakdown of the Meissner state ignited by vortex hot spots is addressed. Section VI concludes with a discussion of the results.

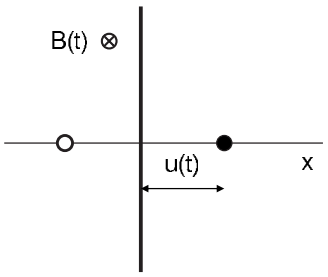

FIG. 1. Vortex (shown as the solid circle) penetrating by the distance $u(t)$ from the semi-infinite surface ($x \geq 0$) exposed to a uniform parallel rf field $B(t)$. The open circle shows the position of the antivortex image.

II. PENETRATION OF A VORTEX OVER THE OSCILLATING SURFACE BARRIER

A. Dynamic equations and time scales

Penetration of vortices in a superconductor is controlled by the Bean-Livingston surface barrier, which results from a competition between the Meissner screening currents pushing the vortex in a superconductor and the attraction force between a vortex and the surface.[37] This surface barrier oscillates under the rf field, so motion of a vortex in and out of a superconductor is described by a dynamic equation. We consider here a type-II superconductor within the London theory, assuming that the rf field $B(t) = B_0 \sin \omega t$ of amplitude B_0 and frequency ω is applied parallel to the flat surface of a superconductor as shown in Fig. 1. Then the equation of motion for a single vortex driven by the rf Meissner current balanced by the image attraction force and the viscous drag force takes the form

$$\eta_0 \dot{u} = \frac{\phi_0 B_0}{\mu_0 \lambda} e^{-u/\lambda} \sin \omega t - \frac{\phi_0^2}{2\pi\mu_0 \lambda^3} K_1\left[\frac{2}{\lambda}\sqrt{u^2 + \xi_s^2}\right], \quad (1)$$

where $u(t)$ is the distance of the vortex core from the surface, λ is the London penetration depth, $\eta_0 = \phi_0 B_{c2}/\rho_n$ is the Bardeen-Stephen vortex viscosity, ρ_n is the normal-state resistivity, ϕ_0 is the magnetic flux quantum, $B_{c2} = \phi_0/2\pi\xi^2$ is the upper critical field, and $K_1(x)$ is the modified Bessel function. Here we introduce the local coherence length ξ_s at the point of the vortex entry, which provides the cutoff in the London theory. For $u < \xi_s$, the last term in Eq. (1) gives a constant force of vortex attraction to the surface due to the formation of a "core string" of depressed order parameter revealed by computer simulations of the GL equations.[16,46]

In this work we treat the emergence of the vortex phenomenologically, assuming that it first appears in a small defect region at the surface. For the results presented below, the actual nature of the defect is not important as long as the defect size is much smaller than λ and the local ξ_s is larger than the bulk coherence length ξ. The vortex penetrates at the field $B(t) > B_v$ for which the local surface barrier disappears

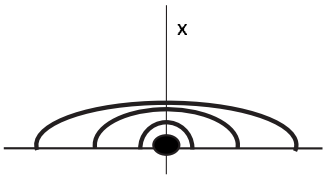

FIG. 2. Snapshots of an expanding vortex semiloop emerging from a surface defect (black dot). The quicker expansion of the loop along the surface is due to the gradient of the Meissner current $J(x) \propto \exp(-u/\lambda)$ and the LO instability.

because the peak Meissner force $\phi_0 B_0/\mu_0\lambda$ exceeds the maximum attraction force to the surface $\phi_0^2 K_1(2\xi_s/\lambda)/2\mu_0\lambda^3$. For $\xi_s \ll \lambda$, we can expand $K_1(x) \approx 1/x$ and obtain

$$B_v = \phi_0/4\pi\lambda\xi_s \approx 0.71 B_c, \tag{2}$$

which basically defines ξ_s in terms of the observed local penetration field B_v, which has been calculated for different types of surface defects.[38–41] We assume that there is a distribution of sparse small regions with reduced local B_v on the surface where vortices first enter. Penetration of straight vortices can only be initiated by linear defects (for example, dislocations or grain boundaries) parallel to the vortex line. For more common three-dimensional (3D) surface defects, such as precipitates or local variation of chemical composition, a vortex first emerges as a semiloop, which then expands as illustrated by Fig. 2. The initial penetration of a small vortex semiloop of radius $R(t) \ll \lambda$ can be described by the following dynamic equation:

$$\eta_0 \dot{R} = \frac{\phi_0 B_0}{\mu_0 \lambda} \sin \omega t - \frac{\epsilon}{R}, \tag{3}$$

where $\epsilon \simeq (\phi_0^2/4\pi\mu_0\lambda^2)\ln(R/\xi)$ is the nonlocal vortex line tension.[42] To the accuracy of the logarithmic factor $\ln(R/\xi) \sim 1$, Eq. (3) reduces to Eq. (1) for a straight vortex displaced from the surface by $u \simeq R \ll \lambda$. Moreover, the circular vortex semiloop very quickly evolves into a loop strongly elongated along the surface because of the gradient of the Meissner current, $J(x) = (B_0/\mu_0\lambda)\exp(-u/\lambda)$, and the LO instability, which effectively straightens the vortex due to jumpwise lateral propagation of the loop, as shown below. As the vortex penetrates in a superconductor, the role of the vortex curvature on the relevant scales $\sim\lambda$ rapidly diminishes, so Eq. (1) can be used after a short transient time, which is still much smaller than the rf period.

Equation (2) gives B_v close to the superheating field $B_s = 0.745 B_c$, above which the Meissner state in extreme type-II superconductors with $\kappa = \lambda/\xi \gg 1$ becomes absolutely unstable with respect to weak periodic perturbations of the order parameter[43–48] as the Meissner current density at the surface $B_v/\mu_0\lambda$ exceeds the local depairing current density J_d. For $B_0 > B_v$, a vortex moves in and out the superconductor under the action of the rf field. Since Eq. (1) can only be used on the scales $u(t) > \xi_s$, we neglect here a possible dependence of η_0 on u, although this dependence can occur if a long-range interaction of the vortex core with the surface due to nonequilibrium effects is taken into account, as shown below.

To estimate the scale of vortex oscillations and maximum velocities, we first disregard the image attraction force, which becomes negligible at distances $u > \lambda$. Then the solution of Eq. (1) takes the form

$$u(t) = \lambda \ln\left[1 + \frac{\phi_0 B_0}{\lambda^2 \omega \eta_0 \mu_0}(\cos \omega t_0 - \cos \omega t)\right], \tag{4}$$

where $t_0 = \sin^{-1}(B_v/B_0)/\omega$ is the time of vortex entry. The maximum vortex penetration depth u_m corresponds to $\cos \omega t = -1$, from which

$$u_m = \lambda \ln\left[1 + \frac{\phi_0}{\lambda^2 \omega \eta_0 \mu_0}(\sqrt{B_0^2 - B_v^2} + B_0)\right]. \tag{5}$$

Here u_m depends logarithmically on the rf field and frequency. From Eq. (4) we estimate the time τ for the vortex to move by the distance $\simeq\lambda$ from the surface. For GHz frequencies and the materials parameters of Nb and Nb_3Sn, τ turns out to be much shorter than the rf period, so $\cos \omega(t_0 + \tau) \simeq \cos \omega t_0 - \omega\tau \sin \omega t_0$; hence,

$$\tau = \frac{\mu_0 \lambda^2 \eta_0}{\phi_0 B_v} \simeq \frac{2\mu_0 \lambda^3}{\rho_n \xi}. \tag{6}$$

Taking $\rho_n = 0.2\ \mu\Omega$ m, $\lambda = 90$ nm, and $\xi = 3$ nm for Nb_3Sn,[49] we obtain $\tau \simeq 3 \times 10^{-12}$ s and $\omega\tau \simeq 0.04$ for 2 GHz. Likewise, taking $\rho_n = 10^{-9}\ \Omega$ m and $\lambda = \xi = 40$ nm for Nb yields $\tau = 4 \times 10^{-12}$ s. Equation (6) gives the lower limit for τ because the image vortex attraction increases τ. For these parameters, τ turns out to be of the order of the time of formation of the vortex core at the surface $\hbar/\Delta$.[14–17]

Now let us consider rf vortex dynamics in more detail. During the positive rf half-period, the vortex penetration starts once $B(t)$ exceeds the local B_v. Because the vortex currents flow antiparallel to the Meissner currents at the surface, penetration of the vortex suppresses the local pair-breaking instability. At the time when the rf field almost changes sign, the vortex penetrates by the maximum distance u_m and then it turns around and starts coming back. However, for negative $B(t)$, the current density at the surface $J(0,t)$ is now a sum of the vortex currents and the parallel Meissner rf currents. As a result, when the outgoing vortex reaches the critical distance u_c from the surface, $J(0,t)$ exceeds J_d, causing penetration of an antivortex before the vortex exits. The antivortex is driven into the sample by the Meissner current and by the attraction to the outgoing vortex, to which it annihilates at the distance u_a from the surface. After that the negative $B(t)$ reaches $-B_v$, and a new antivortex penetrates the sample in the same way as the vortex did for the positive cycle, except that once the antivortex reaches u_c on the way out, it creates a vortex at the surface, both annihilating at u_a. This process repeats periodically.

Equation (1) therefore describes vortex penetration and exit until the Meissner current density plus the current density of the outgoing vortex being at $x = u_c$ reaches $-B_v/\mu_0\lambda$ at the surface at the time $t = t_c$ defined by

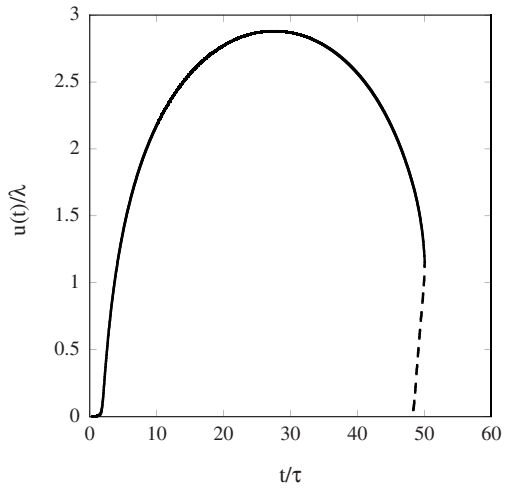

FIG. 3. Dynamics of vortex penetration and exit calculated from Eq. (1) for $t<t_c$ and Eqs. (8) and (9) for $t>t_c$ for $\omega\tau=0.061$ and $B_0=1.01B_v$. The solid and dashed curves show the trajectories of the vortex and antivortex, respectively.

$$B_0|\sin \omega t_c| + \frac{\phi_0}{\pi\lambda^2}K_1\left(\frac{u_c}{\lambda}\right) = B_v. \tag{7}$$

The second term on the left-hand side (lhs) of Eq. (7) results from the equal contributions of the outgoing vortex and its antivortex image to the surface current density $J(0,t)$. For $t>t_c$, the vortex with the coordinate $u_+(t)$ and the antivortex with the coordinate $u_-(t)$ move toward each other, as described by the following equations:

$$\eta_0\dot{u}_+ = \frac{\phi_0 B_0}{\mu_0\lambda}e^{-u_+/\lambda}\sin \omega t - \frac{\phi_0^2}{2\pi\mu_0\lambda^3}\left[K_1\left(\frac{2u_+}{\lambda}\right) + K_1\left(\frac{u_+-u_-}{\lambda}\right) - K_1\left(\frac{u_++u_-}{\lambda}\right)\right], \tag{8}$$

$$\eta_0\dot{u}_- = -\frac{\phi_0 B_0}{\mu_0\lambda}e^{-u_-/\lambda}\sin \omega t - \frac{\phi_0^2}{2\pi\mu_0\lambda^3}\left[K_1\left(\frac{2}{\lambda}\sqrt{u_-^2+\xi_s^2}\right) - K_1\left(\frac{u_+-u_-}{\lambda}\right) - K_1\left(\frac{u_++u_-}{\lambda}\right)\right]. \tag{9}$$

These equations reflect the balance of interaction forces between the vortex and antivortex and their corresponding images similar to those in Fig. 1. The first term on the rhs of Eq. (9) has the minus sign because the Meissner current drives the antivortex in the opposite direction as compared to the vortex. The initial conditions for Eqs. (8) and (9) are $u_+(t_c)=u_c$ and $u_-(t_c)=0$, and the condition $u_+(t_a)=u_-(t_a)=u_a$ defines the annihilation distance u_a and time t_a.

The dynamics of vortex penetration and annihilation is illustrated by Fig. 3 where the vortex penetration depth is $u_m\simeq 3\lambda$, the critical distance is $u_c\simeq 2\lambda$, and the vortex-antivortex annihilation occurs at $u_a\simeq\lambda$. For $\omega\tau\ll 1$, the vortex first accelerates rapidly, penetrating by the distance $\simeq\lambda$ during a time $\sim\tau$, and then slowly turns around during the time of the order of the rf period and annihilates in a short time $\sim\tau$.

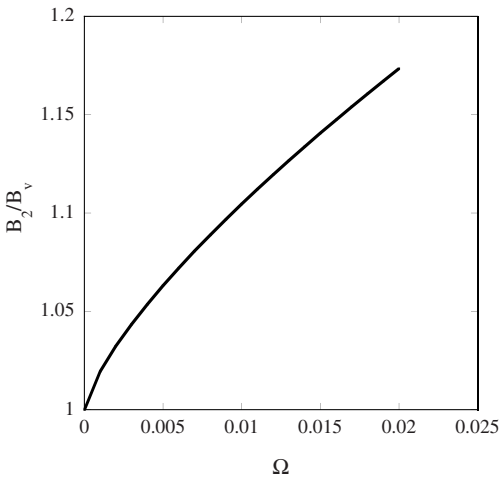

FIG. 4. Dependence of the second-vortex penetration field B_2 on the dimensionless frequency $\Omega=\omega\tau/\kappa$.

The above results are limited to the field region $B_v<B_0<B_s$ where single vortices penetrate independently through regions where the Bean-Livingston barrier is locally suppressed by surface defects separated by distances $>\lambda$. The case $B_0>B_s$ corresponds to a global pair-breaking instability causing multivortex avalanche penetration. Yet even for $B_v<B_0<B_s$, a multivortex chain penetration is possible. Indeed, penetration of a single vortex for $B(t)>B_v$ suppresses the local pair-breaking instability at $x=0$. However, as $B(t)$ increases, the Meissner current density increases, while the counterflow of surface current density at $x=0$ from the vortex decreases as it moves further away from the surface. As a result, $J(0,t)$ can again reach J_d, causing a penetration of the second vortex at $t=t_2$ when the first vortex is located at $x=u_2$ The condition of the second vortex penetration is similar to Eq. (7),

$$B_2\sin \omega t_2 - \frac{\phi_0}{\pi\lambda^2}K_1\left(\frac{u_2}{\lambda}\right) = B_v, \tag{10}$$

except for the minus sign on the lhs Equations (1) and (10) define the critical rf amplitude B_2 below which only the single-vortex penetration occurs. Shown in Fig. 4 is the curve $B_2(\omega)$ obtained by the numerical solution of Eqs. (1) and (10) for Nb_3Sn. These results can be described well by the power-law dependence

$$B_2=[1+p\Omega^\alpha]B_v, \quad \Omega=2\mu_0\lambda^2\omega/\rho_n, \tag{11}$$

where $\Omega=\omega\tau/\kappa$, $\alpha=0.73$, and $p=0.23$. For $\Omega\ll 1$, the field B_2 is close to B_v; however, dissipation produced by penetrating vortices can significantly reduce both B_v and B_2 (see below).

B. Vortex dissipation

The power $Q=(\omega\eta/2\pi)\oint v^2dt$ dissipated due to the work of the viscous drag forces is given by

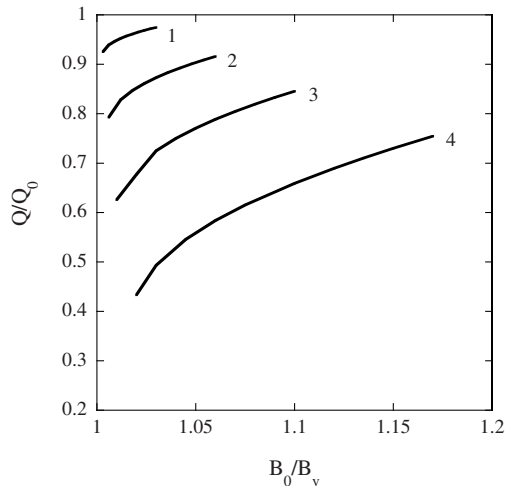

FIG. 5. Dissipated power Q as a function of the rf amplitude in the region of the single-vortex penetration $B_v < B_0 < B_2$ for different frequencies $\omega\tau$: 0.061 (1), 0.162 (2), 0.325 (3), and 0.65 (4). Here $Q_0 = 2\omega\phi_0 B_v/\pi\mu_0$.

$$Q = \frac{\omega\eta}{\pi}\left[\int_{t_0}^{t_c} \dot{u}^2 dt + \int_{t_c}^{t_a} (\dot{u}_+^2 + \dot{u}_-^2) dt\right], \tag{12}$$

where $u(t)$ is the solution of Eq. (1), which describes the dynamics of a single vortex driven by a rf field until $t = t_c$ when the antivortex appears. The second integral in Eq. (12) is due to the collapse of the vortex-antivortex pair described by Eqs. (8) and (9). For a quasistatic field, Q can be obtained from the change of the vortex thermodynamic potential $G(u)$:

$$G(u) = \frac{\phi_0}{\mu_0}\left[B_{c1} - B + Be^{-u/\lambda} - \frac{\phi_0}{4\pi\lambda^2} K_0\left(\frac{2u}{\lambda}\right)\right], \tag{13}$$

where $B_{c1} = \epsilon\mu_0/\phi_0$ is the lower critical field and ϵ is the vortex self-energy. If the ac field $B(t)$ varies very slowly ($\Omega \ll 1$), the dissipated energy equals the sum of $\Delta G_+ = G(0) - G(u_m)$ during the positive half-cycle and $\Delta G_- = G(u_m) - G(0)$ during the negative half-cycle. For any closed vortex trajectory, which starts and ends at the surface, contributions to Q due to vortex self-energy and the work $\oint F_i(u)\dot{u}dt$ of the potential image force $F_i(u)$ vanish. Thus, Q is only determined by the work of the driving Lorentz force, $\simeq (2\phi_0 B_v/\mu_0)[1 - \exp(-u_m/\lambda)]$, for both vortex and antivortex cycles, where we took account of fact that the main contribution to Q comes from the initial acceleration of the vortex during time $\sim\tau$ when the field $B(t)$ is close to B_v. Neglecting $\exp(-u_m/\lambda) \ll 1$, we have

$$Q = 2\omega\phi_0 B_v/\pi\mu_0, \quad \Omega \to 0. \tag{14}$$

The field region of the single-vortex penetration $B_v < B_0 < B_2$ defined by Eq. (11) shrinks as the frequency decreases. In this narrow field region the effect of vortex viscosity can radically change the dependence of Q on B_0 and ω. Shown in Fig. 5 are the results of numerical solution of Eqs. (1)–(9) and (12) for different frequencies and the GL parameter $\kappa = \lambda/\xi_s = 34$. These data are described well by the following formula:

$$Q = \frac{2\omega\phi_0 B_v}{\pi\mu_0}\left(\frac{B_0^2 - B_v^2}{B_v^2}\right)^{\omega\tau_2}, \quad \tau_2 = 3.98\tau\kappa^{-2/3}, \tag{15}$$

which reduces to Eq. (14) for $\omega \to 0$. As follows from Fig. 5 and Eq. (15), the power Q decreases as ω increases because of retardation effects due to vortex viscosity during the short fraction of the rf period in which $B(t) > B_v$.

III. INSTABILITIES AT HIGH rf FIELDS

Once the field $B(t)$ exceeds B_v, the vortex rapidly accelerates, reaching the maximum velocity $v_m \simeq \lambda/\tau$:

$$v_m = \rho_n/2\mu_0\kappa\lambda. \tag{16}$$

Equation (16) gives $v_m \simeq 30$ km/s for Nb_3Sn and $v_m \simeq 10$ km/s for Nb. Not only are the so-obtained values of v_m much higher than the velocity of sound, they may even exceed the critical BCS pair-breaking velocity,[1]

$$v_\Delta = \frac{\Delta}{mv_F} = \frac{\hbar}{\pi m\xi}, \tag{17}$$

where $\xi = \hbar v_F/\pi\Delta$, v_F is the Fermi velocity, and m is the electron mass. Indeed, taking $\xi = 40$ nm and the free electron mass m, we obtain $v_\Delta = 0.8$ km/s $< v_m$ for Nb and $v_\Delta = 10$ km/s $< v_m$ for $\xi = 3$ nm in Nb_3Sn. Here we use the Bardeen-Stephen model for qualitative estimates only, ignoring many still not well understood mechanisms essential at low temperatures—for example, the effect of quantized electron states in the core and the core shrinkage due to the Kramer-Pesch effect,[50] resulting in the factor $\sim\ln(T_c/T)$ in the Bardeen-Stephen formula.[2,51,52] Yet for strong rf fields $B_0 \sim B_c$, the linear viscous drag force derived for small vortex velocities becomes inadequate. It was first predicted theoretically[23] and observed in many experiments[25–30] that the dependence of η on v at high vortex velocities results in a nonmonotonic viscous drag force $f_v = v\eta(v)$ and jumpwise instabilities.

A. Instabilities of viscous flux flow

A nonlinear viscous drag force was first calculated by Larkin and Ovchinnikov,[23] who showed that nonequilibrium effects in the vortex core decrease the drag coefficient η as v increases:

$$\eta(v) = \frac{\eta_0}{1 + v^2/v_0^2}, \tag{18}$$

where η_0 is the Bardeen-Stephen viscosity. The critical velocity v_0 in the dirty limit is given by

$$v_0 \simeq 0.6\left(\frac{\ell_i v_F}{\tau_\epsilon}\right)^{1/2}\left(1 - \frac{T}{T_c}\right)^{1/4}. \tag{19}$$

Here ℓ_i is the mean free path due to impurities and $\tau_\epsilon(T)$ is the quasiparticle energy relaxation time. Equation (18) re-

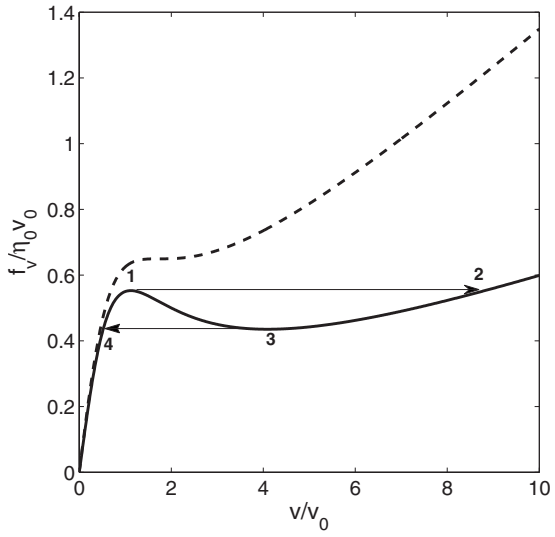

FIG. 6. The viscous drag force $f_v(v)$ as a function of the vortex velocity for the LO instability. The dashed curve shows $f_v(v)$ at $\eta_0=8\eta_i$. For $\eta_0>8\eta_i$, an N-shaped dependence $f_v(v)$ develops, as illustrated by the solid curve plotted for $\eta_i=0.05\eta_0$. The arrows show the jumpwise change of $v(F)$, as the driving force F increases above the maximum value of $f_v(1)$ and then decreases below the minimum value $f_v(3)$.

sults in a nonmonotonic dependence of the viscous drag force, $f_v=v\eta(v)$, on the vortex velocity:

$$f_v(v)=\frac{\eta_0 v}{1+v^2/v_0^2}+\eta_i v. \tag{20}$$

Here, following the LO approach, we use two effective viscosities η_0 and η_i, where η_i phenomenologically takes into account the transition to the normal state as v reaches the pair-breaking velocity v_Δ. For $\eta_0>8\eta_i$ an N-shaped dependence $f_v(v)$ develops, as shown in Fig. 6. For $\eta_i=0$, the drag force reaches the maximum value $F_m=\eta_0 v_0/2$ at $v=v_0$.

The LO instability was originally associated with acceleration of normal quasiparticles in the vortex core by an electric field, which can increase their energy above Δ. In this case quasiparticles can escape the core if the diffusion length $L_D=(D\tau_\epsilon)^{1/2}$ exceeds the core size. The resulting quasiparticle depletion in the core reduces the core size and the vortex viscosity according to Eqs. (18) and (19). However, Eq. (18) is actually more general and may result from several different mechanisms. In particular, the velocity dependence (18) can result from coupling of the vortex motion with other diffusion process, including quasiparticle or temperature diffusion around the moving vortex core. For example, the electron overheating of the core can lead to Eq. (18) as follows.

The power ηv^2 generated by the viscous drag increases the electron temperature in the core T_m, reducing the vortex viscosity $\eta(T_m)\propto B_{c2}(T_m)$. Linearizing $\eta(T_m)\simeq\eta_0(1-T_m/T_c)$, we write the thermal balance condition

$$(T_m-T_0)g=\eta_0(1-T_m/T_c)v^2, \tag{21}$$

where $g\sim\pi k/\ln(L_\theta/L_\xi)$ defines the heat flux from the core due to the thermal conductivity $k(T)$, where the thermal length L_θ is of the order of the film thickness d for ideal cooling and $L_\xi\sim\sqrt{\xi\lambda}$ is the length related to the amplitude of vortex penetration. This logarithmic factor will be calculated in the next section in more detail; here we just use $\ln(L_\theta/L_\xi)\sim\ln(d/\sqrt{\xi\lambda})$ for qualitative estimates. Solving Eq. (21) for T_m results in the velocity-dependent $\eta(T_0)$ of the LO form:

$$\eta=\eta_0(1-T_0/T_c)/(1+\eta_0 v^2/g), \tag{22}$$

$$v_0=(g/\eta_0)^{1/2}\sim[\pi k\rho_n/\phi_0 B_{c2}(0)\ln(L_\theta/L_\xi)]^{1/2}. \tag{23}$$

Substituting here the low-T quasiparticle thermal conductivity $k\sim k_n(\Delta/T)^2\exp(-\Delta/T)$ and using the Wiedemann-Frantz law $k_n\rho_n=(\pi k_B/e)^2T/3$, and $B_{c2}(0)\sim\phi_0/2\pi\xi_0\ell_i$ and $\xi_0\sim\hbar v_F/\Delta$ in the dirty limit, we reduce Eq. (23) to Eq. (19). Here the time constant

$$\tau_\epsilon\sim\frac{\hbar T}{\Delta^2}\ln\left(\frac{L_\theta}{L_\xi}\right)\exp\left(\frac{\Delta}{T}\right) \tag{24}$$

exhibits an exponential temperature dependence similar to the energy relaxation time τ_ϵ between quasiparticles and phonons[53] in the LO theory. However, the exponential dependence of $\tau_\epsilon(T)$ in the thermal model is cut off at lower T where k is limited by phonons.

To estimate v_0, we take $\rho_n=0.2\ \mu\Omega$ m, $k=10^{-2}$ W/mK, $B_{c2}=23$ T for Nb_3Sn at low temperatures[49] and $L_\xi\sim\sqrt{\lambda\xi}\sim16$ nm, $L_\theta\sim d\sim1$ mm, and $\ln(L_\theta/L_\xi)\sim11$. For these parameters, Eq. (23) gives $v_0\sim0.1$ km/s, much smaller than the estimates for v_Δ and v_m. Thus, overheating does result in the same equation (18), although in this case the vortex core expands as it becomes warmer at higher velocities,[35,36] in contrast to the LO core shrinkage. The critical velocity v_0 defined by Eq. (23) remains constant at T_c, unlike vanishing $v_0(T_0)$ for the LO mechanism, which thus dominates at $T\approx T_c$. For $T\to T_c$, both Eqs. (19) and (23) give the critical velocity $v_0(T)$, which exceeds the linear viscous-drag-limited velocity $v_m(T)\propto(1-T/T_c)^{1/2}$ given by Eq. (16). Thus, Eq. (1) adequately describes rf vortex dynamics at strong fields $B_0\sim B_c$ and temperatures close to T_c.

To evaluate the overheating mechanism in more detail, we assume that $\eta(T_m)$ depends on a local electron temperature $T_m(t)$ in the vortex core. The distribution of $T(\mathbf{r},t)$ around a moving vortex is described by a thermal diffusion equation

$$C\dot{T}=k\nabla^2T-\alpha(T-T_0)+\eta(T_m)v^2(t)f(x-u(t),y), \tag{25}$$

which, after redefinition of the coefficients, can be reduced to the same mathematical form as the diffusion equation for nonequilibrium quasiparticles. Here C is the heat capacity, k is the thermal conductivity, $u(t)$ is the coordinate of the vortex core moving with velocity $v(t)$, and the function $f(x,y)$ accounts for the finite core size, so that $\int f(r)d^2r=1$. The term $\alpha(T-T_0)$ describes heat exchange with the environment. For example, $\alpha=h/d$ in a thin film of thickness d where h is the Kapitza conductance at the sample surface and T_0 is the bath temperature. For electron overheating, the parameter $\alpha=C/\tau_\epsilon$ describes heat exchange between electrons and the lattice, where C is the electron specific heat and τ_ϵ is the time

of inelastic scattering of quasiparticles in the vortex core on phonons.[36,53–55] The last term on the rhs of Eq. (25) describes dissipation in the vortex core proportional to the viscosity $\eta(v,T_m)$ taken at the local core temperature $T_m(t)$, which, in turn, depends on $v(t)$. The core form factor $f(r)$ is modeled by the Gaussian function $f(r)=\pi^{-1}\xi_1^{-2}\exp(-r^2/\xi_1^2)$, where the core radius ξ_1 can be smaller than ξ at $T\ll T_c$ due to the Kramer-Pesch effect[50] [the solutions of Eq. (25) depend weakly on ξ_1]. We also consider weak overheating for which the dependences of C, k, and α on T can be neglected. As shown below, T can be regarded as either the electron or the lattice temperature, depending on the time scale of the vortex dynamics involved.

The solution of Eq. (25), given in Appendix A, results in the following integral equation for the temperature $T_m(t)$ in the vortex core moving with a time-dependent velocity $v(t)$ near the surface:

$$T_m(t)=T_0+\frac{1}{\pi k}\int_0^\infty \frac{dt' q(t-t')e^{-t'/t_\theta}}{4t'+t_s}\times\left\{\exp\left[-\frac{[u(t)-u(t-t')]^2}{(4t'+t_s)D}\right]\pm\exp\left[-\frac{[u(t)+u(t-t')]^2}{(4t'+t_s)D}\right]\right\}, \tag{26}$$

where $q(t)=\eta(T_m(t),v(t))v^2(t)$ is the time-dependent power generated by the moving vortex, $D=k/C$ is the thermal diffusivity, $t_s=\xi_1^2/D$ is the diffusion time across the vortex core, and $t_\theta=C/\alpha$ is the electron energy relaxation time. The second term in the parentheses describes the effect of the surface: the plus sign corresponds to the thermally insulated surface, $\partial_x T(x,t)|_{x=0}=0$, and the minus sign corresponds to the ideal cooling, $T(0,t)=T_0$. Here we do not consider microscopic thermal gradients inside the vortex core,[56] assuming that their effect is included in the bare η. Equation (26) is written for steady-state vortex oscillations, so that the rf field was turned on at $t_i=-\infty$ and $v(t)$ in Eq. (26) accounts for all oscillations preceding the time t.

The integral, Eq. (26), takes into account retardation effects due to a diffusive redistribution of $T(\mathbf{r},t)$ around an accelerating vortex, so $T_m(t)$ depends on the vortex velocity $v(t-t')$ at earlier times. The effect of the surface makes $T_m(t)$ dependent on the vortex coordinate $u(t)$ as well. Equation (26) simplifies considerably if $v(t)$ varies slowly over the relaxation time t_θ, and $t_s\ll t_\theta$ and $u(t)>\xi_1$. Then $q(t-t')$ can be taken out of the integral at $t'=0$, and Eq. (26) yields the following equation for the local temperature difference $\delta T_m=T_m-T_0$:

$$\delta T_m=\frac{\eta(T_m)v^2}{2\pi k}\left[\ln\frac{L_\theta}{\tilde{\xi}}\pm K_0\left(\frac{2u}{L_\theta}\right)\right]. \tag{27}$$

Here $\tilde{\xi}=\xi_1 e^{\gamma/2}/2\approx 0.67\xi_1$ and $\gamma=0.577$ is the Euler constant.[57] The second term in the parentheses decreases exponentially for $u>L_\theta$, and logarithmically, $K_0(z)\simeq\ln(2/z)-\gamma$ for $\tilde{\xi}\ll u\ll L_\theta$. In this case the expression in the parentheses reduces to $\ln(L_\theta/\tilde{\xi})+\ln(L_\theta/\tilde{u})$, where $\tilde{u}=ue^\gamma/2$. Taking the characteristic amplitude of vortex penetration, $\tilde{u}\sim\lambda$, we can present the logarithmic part in the form $2\ln(L_\theta/L_\xi)$, where $L_\xi=(\tilde{u}\tilde{\xi})^{1/2}\sim\sqrt{\tilde{\xi}\lambda}$ was used before to obtain Eq. (18) in the thermal model. The weak logarithmic dependence of v_0 on L_ξ and L_θ makes Eq. (23) nearly insensitive to the details of heat transfer and the behavior of $u(t)$.

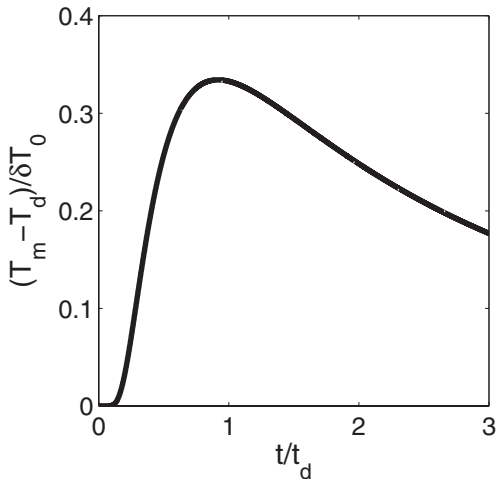

FIG. 7. Temperature spike in the vortex core after the jump described by Eq. (28) for $t_\theta=10t_d$, $t_d=\delta u^2/4D$, $\delta T_0=WD/\pi k\delta u^2$, and $T_d=T_0+\eta_0 v_0^2\ln(L_\theta/\tilde{\xi})/2\pi k$.

In the other limiting case of a very rapid variation of $v(t)$, the vortex reaches the critical velocity v_0 and then jumps by the distance δu, dissipating the energy W during the short time δt. Then $q(t)=q_0+W\delta(t)$ and Eq. (26) results in the following implicit equation for $\delta T_m(t)$ at $t>\delta t$:

$$\delta T_m(t)\simeq\frac{\eta_0 v_0^2}{2\pi k}\ln\frac{L_\theta}{\tilde{\xi}}+\frac{W(T_m)}{4\pi kt}e^{-\delta u^2/4Dt-t/t_\theta}, \tag{28}$$

which describes a temperature spike in the core followed by relaxation of $\delta T_m(t)$, as shown in Fig. 7. Here the first term on the rhs gives δT_m before the jump and the effect of the surface is neglected.

Next we consider the steady-state temperature field $T(\mathbf{r})$ averaged over rf oscillations, where $T(\mathbf{r})$ is determined by the balance of the vortex heat source and thermal diffusion. Solution of the thermal diffusion equation in Appendix A yields the following distribution of $\delta T(\mathbf{r})=T(\mathbf{r})-T_0$ from a heat source localized at the thermally insulated surface ($x=0$) of a slab of thickness d, ideally cooled from the other side, $\delta T(d)=0$:

$$\delta T(\mathbf{r})=\frac{1}{2\pi k}\int_0^d q(x')\ln\frac{\cosh\frac{\pi y}{2d}+\cos\frac{\pi(x+x')}{2d}}{\cosh\frac{\pi y}{2d}-\cos\frac{\pi(x-x')}{2d}}dx'. \tag{29}$$

Here $q(x)$ is the power density averaged over the rf period. On scales greater than the size of the heat source, $\delta T(\mathbf{r})$ depends only on the total power $Q=\int_0^d q(x)dx$:

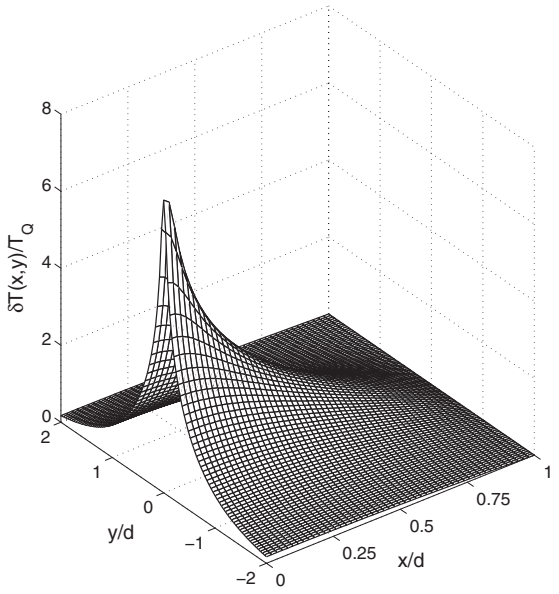

FIG. 8. Temperature variation $\delta T(x,y)=T(x,y)-T_0$ around a heat source given by Eqs. (29) and (30) for $u_m=10^{-3}d/\pi$ and normalized by $T_Q=Q/2\pi k$.

$$\delta T(\mathbf{r}) = \frac{Q}{2\pi k} \ln \frac{\cosh(\pi y/2d) + \cos(\pi x/2d)}{\cosh(\pi y/2d) - \cos(\pi x/2d)}. \tag{30}$$

Here $\delta T(\mathbf{r})$ decays exponentially over the length $2d/\pi$ as shown in Fig. 8. Near the heat source $\delta T(\mathbf{r})$ weakly (logarithmically) depends on details of $q(x)$. As shown in Appendix A, the distribution of $\delta T(0,y)$ along the surface to the logarithmic accuracy is given by

$$\delta T(0,y) = \frac{Q}{2\pi k} \ln \frac{16d^2}{\pi^2(y^2+r_0^2)}, \quad y^2 \ll d^2, \tag{31}$$

where r_0 quantifies the size of a dissipation source. The account of finite r_0 cuts off the logarithmic divergence in Eq. (30) at $x=y=0$, resulting in a maximum temperature disturbance at $y=0$:

$$\delta T_m \simeq \frac{Q}{\pi k} \ln \frac{4d}{\pi r_0}. \tag{32}$$

Equation (32) reduces to Eq. (27) with $u \sim r_0$ and $L_\theta \sim d$.

The physical meaning of T in the above formulas depends on the relevant vortex time scales. For example, for the supersound vortex penetration or vortex jumps on a time scale much shorter than the electron-phonon energy relaxation time, the quasiparticles are not in equilibrium with the lattice and $T(\mathbf{r},t)$ in Eq. (28) can be regarded as an electron core temperature. However, steady-state vortex oscillations in the rf field generate a dc power, which must be transferred to the coolant through phonons. In this case Eqs. (29) describes the lattice temperature distribution around a vortex if the phonon mean free path is shorter than the film thickness.[24] Thus, the vortex oscillates in a "warm tunnel" with the lattice temperature $\delta T(\mathbf{r})$ shown in Fig. 8, but in addition to that the vortex core gets overheated with respect to the lattice during short periods of rapid acceleration, jumps, or annihilation with antivortices, as described before.

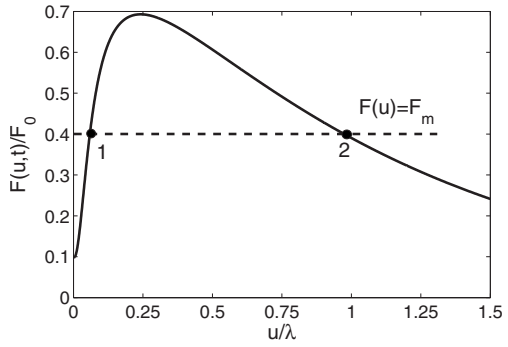

FIG. 9. Instantaneous profile of the force $F(u)$ normalized by $F_0=\phi_0 B_v/\mu_0\lambda$ for $B(t)=1.1B_v$ and $\kappa=20$. The dashed line shows the maximum viscous force $F_m=\eta_0 v_0/2$, which can balance $F(u)$ only in the regions where $F(u)<F_m$. Thus, the vortex first moves from $u=0$ to $u=u_1$, then jumps from point 1 to point 2, after which it moves continuously as described by Eq. (33) until the next jump and annihilation with the antivortex on the way back.

B. Jumpwise vortex penetration

For the LO vortex drag coefficient $\eta(v)$ given by Eq. (18), the equation of motion becomes

$$\frac{\eta_0 \dot{u}}{1+\dot{u}^2/v_0^2} = \frac{\phi_0 B_0}{\mu_0 \lambda} e^{-u/\lambda} \sin \omega t - \frac{\phi_0^2}{2\pi\mu_0\lambda^3} K_1\left[\frac{2}{\lambda}\sqrt{u^2+\xi_s^2}\right]. \tag{33}$$

The nonmonotonic velocity dependence of the viscous drag force on the lhs of Eq. (33) qualitatively changes the vortex dynamics as $v(t)$ exceeds the critical value v_0 for which the viscous force reaches the maximum $F_m=\eta_0 v_0/2$. Indeed, the differential equation for $u(t)$ has the form $\eta_0\dot{u}/(1+\dot{u}^2/v_0^2)=F(u,t)$, where F is the net electromagnetic force given by the rhs of Eq. (33). We can introduce the ratio P of the maximum Lorentz driving force at $B_0=B_v$ to the maximum viscous force:

$$P = \frac{2\phi_0 B_v}{\mu_0 \lambda \eta_0 v_0}. \tag{34}$$

As shown above, the Bardeen-Stephen viscous flow results in unphysically high vortex velocities, indicating that $P \gg 1$ and the dependence of η on v must be taken into account. In this case there are regions at the surface where $F(u,t)$ exceeds F_m as shown in Fig. 9. In these regions the force balance equation (33) cannot be satisfied and the vortex jumps to the place where $F(x) \leqslant F_m$. To see how it happens, we present the quadratic equation (33) for $\dot{u}$ in the form

$$\dot{u} = v_\pm(F) = \frac{v_0 F_m}{F(u,t)}\left[1 \pm \sqrt{1-\frac{F^2(u,t)}{F_m^2}}\right], \tag{35}$$

where $F_m=\eta_0 v_0/2$. For $v \ll v_0$ and $F \ll F_m$, Eq. (35) with the minus sign in the brackets reduces to Eq. (1).

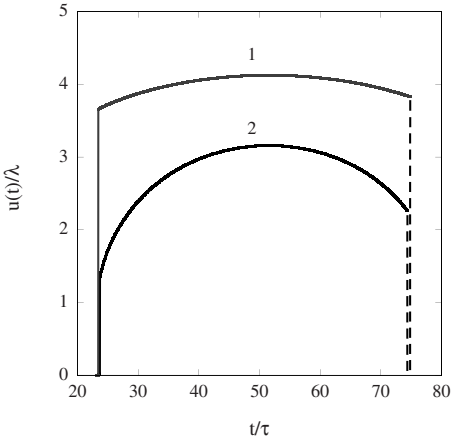

FIG. 10. Jumpwise vortex penetration calculated by solving Eq. (33) for $\kappa=34$, $\omega\tau=0.061$, $B_0=1.02B_v$, and $v_0=0.052v_m$, $P=38.4$ (1) and $v_0=0.52v_m$, $P=3.84$ (2). The dashed lines show the antivortex penetration.

Penetration of the vortex at $B(t)>B_v$ is therefore described by the first-order differential equation $\dot{u}=v_-(F)$, which is well defined only if $F(u,t)\leqslant F_m$; otherwise, the driving force exceeds the maximum friction force and the square root in Eq. (35) becomes imaginary. Vortex dynamics in this case can be understood from Fig. 9, which shows an instantaneous profile of $F(u,t)$ for $B(t)>B_v$. Here a vortex enters the sample with zero velocity at $t=t_0$ and then accelerates because the net force $F(u,t)$ increases as the vortex moves away from the surface and the vortex-image attraction weakens. This part of $u(t)$ is described by the equation $\dot{u}=v_-(F)$ until the vortex reaches the point 1 where $F(u,t)=F_m$. In the region $u>u_1$, the friction force cannot balance the driving force, so the vortex jumps to a point 2 where $F(u,t)=F_m$ and the viscous drag can balance the driving force. As follows from Eq. (28), the core temperature does not change right after the jump ($t\to 0$), but then starts increasing. After that the smooth parts of $u(t)$ are described by the same dynamic equation $\dot{u}=v_-(F)$ for the vortex, which reaches the maximum penetration depth u_m and then turns around and accelerates toward the surface during the negative rf half-period. However, as the vortex reaches the negative critical velocity $-v_0$ on the way out, it jumps again and either exits the sample or collides with the incoming antivortex and annihilates as described in the previous section. The positions of the jumps u_j at the corresponding times $t=t_j$ are determined by the equation $F(u_j,t_j)=\pm F_m$:

$$\pm\frac{\eta_0 v_0}{2}=\frac{\phi_0 B_0 e^{-u_j/\lambda}}{\mu_0\lambda}\sin\omega t_j-\frac{\phi_0^2}{2\pi\mu_0\lambda^3}K_1\left(\frac{2u_j}{\lambda}\right), \quad (36)$$

where the $\pm$ signs should be taken for the incoming and outgoing parts of $u(t)$, respectively. Shown in Fig. 10, are examples of vortex penetration dynamics calculated numerically from Eq. (33). In this case the antivortex jumps in and annihilates with the outgoing vortex before the vortex reaches the critical velocity $-v_0$.

As mentioned above, the LO instability facilitates a quick evolution of the vortex semiloop originating at a 3D surface defect into a straight vortex parallel to the surface. Indeed, as evident from Fig. 2, the vortex propagation velocity is maximum for the segments of the semiloop perpendicular to the surface because they are driven by the continuously increasing maximum Lorentz force $F_L=B(t)\phi_0/\mu_0\lambda$. As a result, the LO instability first occurs for the perpendicular vortex segments, causing them to jump along the surface to the place where the viscous force is able to balance the Lorentz force. Unlike the parallel vortex segments whose jump distance $\sim\lambda$ perpendicular to the surface is limited by the London screening, the jump length along the surface is limited by the lateral sample size. Thus, the vortex semiloop turns into a straight vortex in a jumpwise manner when the lateral velocity of the perpendicular vortex segments reach $\pm v_0$.

Several points should be made regarding the jumpwise vortex dynamics. First, the vortex trajectory $u(t)$ comprised of the jumps connected by smooth parts described by the equation $\dot{u}=v_-(F)$ occurs only if $\dot{F}(u_j,t_j)<0$ at the jump points where $v(t_j)=\pm v_0$. At higher frequencies, or as the vortex overheating is taken into account, there are situations when $\dot{F}(u_j,t_j)>0$. In this case the vortex velocity after the jump exceeds v_0 and the smooth parts of $u(t)$ are described by both branches $\dot{u}=v_\pm(F)$, as shown in Appendix B.

The second point is that, for the overdamped dynamics described by Eq. (33), the jumps occur instantaneously unless the second ascending branch due to the η_i term in Eq. (20) is taken into account. This branch in the LO model corresponds to very high velocities $\sim v_\Delta$, for which an adequate theory of the nonequilibrium vortex core structure and the vortex drag force is lacking. In our phenomenological London approach we assumed that the vortex jumps to the nearest point u_2 where the friction force is able to balance the driving force $F(u_2)=F_m$. However, the instantaneous LO dependence $\eta(v)$ does not include retardation effects due to finite relaxation times of the superconducting order parameter or a diffusive redistribution of nonequilibrium quasiparticles or temperature around a rapidly accelerating or decelerating vortex core. These effects are taken into account by the integral, Eq. (26), for the core temperature $T_m(t)$, which shows that the vortex jump time and length are affected by intrinsic dynamics of η. Thus, there is a diffusion time scale $\delta t\sim\delta u^2/D$ for the vortex jump by the distance δu, where D equals either k/C in the thermal model or the quasiparticle diffusivity in the LO theory. In the thermal model this estimate gives $\delta t\sim 4\times 10^{-12}$ s if we take $\delta u\simeq\lambda=65$ nm, $k\simeq 0.1$ W/mK, and $C\sim 100$ J/m^3 K for Nb_3Sn at 2 K,[49] or even a much shorter time for Nb, for which $\lambda=40$ nm and $\kappa\simeq 10$ W/mK. The so-estimated δt is smaller than the inverse gap frequency, indicating that once the overheated core gets in the region where the friction force is able to balance the driving force, it cools down very quickly due to the electron component of thermal conductivity. In Nb the electron thermal conductivity $k\propto\exp(-\Delta/T)$ is still significant down to $T>1$ K, but at lower temperatures δt may be limited by much slower phonon irradiation from the overheated core. At the same time, the electron temperature relaxation time τ_ϵ outside the core results from a slow phonon-mediated recombination of quasiparticles,[53]

$$\tau_\epsilon \simeq \tau_0\left(\frac{\Delta}{T}\right)^{1/2}\exp\left(\frac{\Delta}{T}\right), \tag{37}$$

which yields $\tau_\epsilon \sim 30$ ns, much longer than the thermal diffusion time δt for Nb at 2 K. For $\omega\tau_\epsilon \gg 1$, the quasiparticles are overheated with respect to the lattice in a highly inhomogeneous way according to the distribution of the lattice temperature $T(\mathbf{r})$ shown in Fig. 8. In this case the condition $\omega\tau_\epsilon(\mathbf{r}) > 1$ of the electron overheating can locally be satisfied in colder regions away from the core, but near the vortex core the electron temperature can be close to the lattice temperature if $\omega\tau_\epsilon(\mathbf{r}) < 1$ because of a higher $T(\mathbf{r})$, which greatly accelerates the energy exchange between electrons and phonons. For example, for Nb at $T_0 = 2$ K, the local increase of the lattice temperature to $T = 4$ K yields $\tau_\epsilon(T) \simeq \tau_\epsilon(T_0)\exp(-\Delta/T_0 + \Delta/T)$, giving $\tau_\epsilon \sim 0.3$ ns and $\omega\tau_\epsilon \sim 1$ at 1–2 GHz.

Another contribution to δt comes from a finite vortex mass M. In the Suhl model $M = 2mk_F/\pi^3$ is due to localized electrons in the vortex core, where $k_F = (3\pi^2 n)^{1/3}$ is the Fermi wave vector.[58] The jump by λ due to the driving force $F = \phi_0 B_v/\mu_0\lambda$ takes the time δt set by the Newton law $2\lambda/\delta t^2 \simeq F$. Using $B_v = \phi_0/4\pi\lambda\xi$, $\lambda^2 = \mu_0 m/ne^2$, and $\xi = \hbar v_F/\pi\Delta$, we obtain

$$\delta t \simeq \frac{4\hbar}{\Delta}\kappa^{1/2}. \tag{38}$$

A more accurate account of quantized levels in the vortex core[59,60] or lattice deformation around the moving vortex[61–63] can increase the vortex mass, thus further increasing the jump time δt. Yet although vortex jumps are quantified by the multiple relaxation times discussed above, they seem to occur much faster than the rf periods we are dealing with in this work.

C. rf dissipation

The power Q dissipated with the account of the jumpwise vortex instabilities can be written in the form

$$Q = \frac{\omega}{\pi}\left\{\oint \eta(\dot{u})\dot{u}^2 dt + \oint \eta(\dot{u})(\dot{u}_1^2 + \dot{u}_2^2)dt + \sum_m [G(t_m, u_{m+}) - G(t_m, u_{m-})]\right\}, \tag{39}$$

where the integrals are taken over all smooth parts of the vortex trajectory $u(t)$, including the vortex-antivortex annihilation parts, like in Eq. (12). The last term in Eq. (39) is the sum of energies released during all vortex jumps at $t = t_m$, from $u = u_{m-}$ to $u = u_{m+}$, where the instantaneous free energy $G(u,t)$ is given by Eq. (13). Shown in Fig. 11 is the second-vortex penetration field B_2 calculated by solving Eqs. (33), (36), and (39) numerically for the parameters of Nb_3Sn. Here B_2 cannot be fit with a power law similar to Eq. (11).

The LO instability makes the behavior of $Q(B_0, \omega)$ more complicated as compared to $Q(B_0)$ described by Eq. (15). As shown in Fig. 12, there are three distinct field regions of very different vortex dynamics. The pure Bardeen-Stephen dynamics like that shown in Fig. 3 is limited to a very narrow region of B_0 close to B_v (labeled by a in the inset). In this case the vortex penetration depth u_m turns out to be smaller than ξ, indicating that the London theory combined with the Bardeen-Stephen drag cannot give a self-consistent description of vortex dynamics at low temperatures. However, Eq. (1) adequately describes the rf vortex dynamics at higher T close to T_c where the LO instability is irrelevant because the

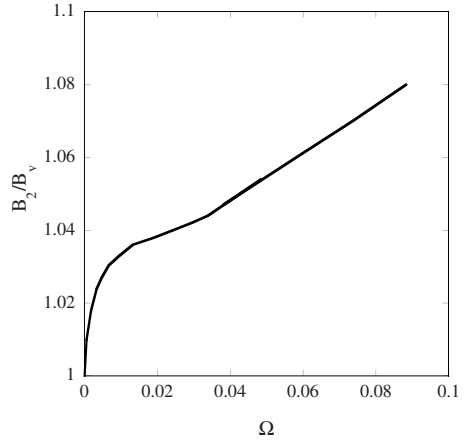

FIG. 11. The dependence of the second penetration field B_2 on the dimensionless frequency $\Omega = \omega\tau/\kappa$ for the LO instability at $\kappa = 34$ and $v_0 = 0.52v_m$.

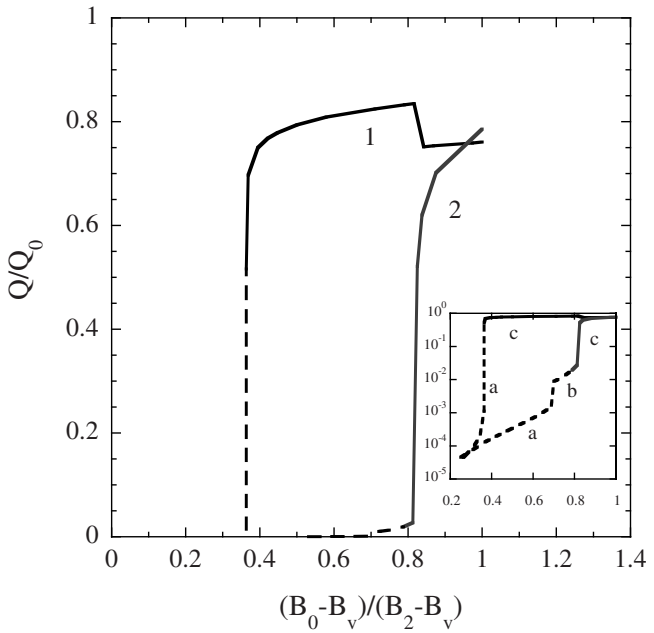

FIG. 12. $Q(B_0)$ calculated with the account of the LO instability for $\kappa = 34$, $v_0 = 0.52v_m$, and $\Omega = 0.019$ (1) and $\Omega = 0.089$ (2). Solid lines show the parts of $Q(B_0)$, for which $u_m > \xi_s$. The inset shows the detailed behavior of $Q(B_0)$ close to B_v, where the parts labeled a correspond to the pure Bardeen-Stephen dynamics for the entire $u(t)$. Parts b are partially controlled by the Bardeen-Stephen drag for the vortex reaching u_m, then turning back and then jumping to the surface from $u = u_c < u_m$ due to the LO instability. Parts c correspond to the LO dynamics similar to that in Fig. 10.

critical velocity $v_0 \propto (1-T/T_c)^{1/4}$ becomes larger than $v_m \propto (1-T/T_c)^{1/2}$.

The parts of the $Q(B_0)$ curves labeled b in Fig. 12 correspond to an intermediate case, for which the most part of $u(t)$, including the initial acceleration of the vortex, reaching the maximum penetration depth u_m, and turning back, does not involve the LO instability. However, as the velocity of the exiting vortex exceeds $-v_0$, it jumps to the surface and disappears, significantly increasing the dissipated power Q. Further increase of B_0 corresponds to the parts of $Q(B_0)$ curves labeled c, for which the LO instabilities occur both on the penetration and the exit parts of $u(t)$, like those in Fig. 10. In this case $Q(B_0)$ jumps up to a much higher level $Q \sim Q_0$ until the second penetration field B_2 is reached. Here the behavior of $Q(B_0)$ can also depend on ω: for lower frequency (curve 1), $Q(B_0)$ increases weakly between $0.4 < \varepsilon(B_0) < 0.8$, but for $\varepsilon = (B_0 - B_v)/(B_2 - B_v) > 0.8$, the power $Q(B_0)$ jumps down. This behavior reflects the change in the vortex dynamics: for $0.4 < \varepsilon < 0.8$, the vortex jumps out of the sample before the antivortex enters, while for $\epsilon > 0.8$, the jump of the vortex toward the surface is accompanied by the penetration of the antivortex and their annihilation, like that in Fig. 10. For higher frequencies, this change in the vortex dynamics formally occurs only for $B_0 > B_2$, so the down step in $Q(B_0)$ does not show up in curve 2 in Fig. 12.

D. Thermal self-localization of vortex penetration

The local temperature increase around an oscillating vortex reduces both critical fields $\tilde{B}_v = B_v(T_m)$ and $\tilde{B}_2 = B_2(T_m)$ as compared to their isothermal values $B_v(T_0)$ and $B_2(T_0)$. To evaluate this effect we combine Eq. (15) for Q and Eq. (32) for T_m and obtain for $\omega\tau_2 \ll 1$

$$\delta T_m \simeq \frac{2\omega\phi_0 B_v}{\pi^2 \mu_0 k} \ln\left(\frac{4d}{\pi r_0}\right). \tag{40}$$

Next we linearize $\tilde{B}_v \simeq B_v - |B_v'|\delta T_m$ with respect to δT_m, where $B_v' = \partial_T B_v(T_0)$. Then the effective fields $\tilde{B}_v$ and $\tilde{B}_2$ take the form

$$\tilde{B}_v = (1-b)B_v, \quad \tilde{B}_2 = (1-b)B_2, \tag{41}$$

$$b = \frac{2\omega\phi_0|B_v'|}{\pi^2\mu_0 k} \ln\left(\frac{4d}{\pi r_0}\right). \tag{42}$$

Both B_2 and B_v are reduced by dissipation, which produces constant shifts of local B_v values but does not change their initial distribution. Taking $k = 10$ W/mK, $B_v' \simeq B_v/T_c$, $B_v = 0.15$ T, $\omega/2\pi = 2$ GHz, and $\ln(4d/\pi r_0) \simeq 10$ for Nb, we obtain $b \sim 3 \times 10^{-2}$, in which case the thermal shift of B_v is negligible. However, for Nb_3Sn, with $\kappa \sim 10^{-2}$ W/mK, the value $b \sim 1$ is much higher, so thermal effects can significantly expand the field region $\tilde{B}_v < B_0 < B_s$ of single-vortex penetration.

The condition of the single-vortex penetration $B_v < B_0 < B_2$ implies that the local value of B_2 is smaller than the uniform superheating field B_s. Multiple-vortex penetration for $B_0 > B_2$ causes strong dissipation, further decreasing B_2 and resulting in avalanche-type dendritic vortex penetration.[64,65] Such thermomagnetic dendritic flux avalanches have been observed in both low-T_c and high-T_c superconductors.[66–71] Notice that the superfast vortex penetration through the surface barrier due to the jumpwise LO vortex instability may pertain to the supersonic vortex velocities observed for dendritic vortex penetration in $YBa_2Cu_3O_7$ and YNi_2B_2C films.[66,71]

The temperature distribution (30) results in the long-range dc repulsion force $\mathbf{f}_T(L) = -s^* \nabla T$ between two oscillating vortices spaced by L. Here $s^*(T)$ is the vortex transport entropy responsible for thermomagnetic effects in the mixed state.[72,73] In thick films $d \gg \lambda$, vortices are localized at the surface, so to calculate the thermal force $f_T(L)$, we put $x=0$ in Eq. (30) and obtain

$$f_T(L) = \frac{s^* Q}{2dk \sinh(\pi L/2d)}. \tag{43}$$

This long-range force on a scale much greater than λ results in repulsion of neighboring vortex penetration channels, facilitating bending instability and dendritic branching of the multivortex tracks.

IV. EFFECT OF PINNING

A. Trapping rf vortices at strong fields, $B_0 \sim B_v$

At the initial stage of vortex penetration, $B(t) \simeq B_v$, the driving force F_L is much stronger than typical pinning forces by materials defects. However, as the vortex moves deeper into the sample, the force $F_L(u) \propto \exp(-u/\lambda)\sin\omega t$ decreases exponentially, so pinning becomes more effective if the vortex trajectory passes a pin aligned with the place of the vortex entry within a "belt" $\sim\lambda$ wide. In this case the vortex can be trapped and stay pinned as the rf field changes sign. As $B(t)$ reaches $-B_v$ during the negative rf cycle, an antivortex penetrates along the same trajectory as the vortex did and annihilates with the pinned vortex.

The power dissipated due to the vortex-antivortex annihilation can be evaluated from the change of the thermodynamic potential $G(u)$:

$$Q \simeq \frac{\omega B_v}{\pi\phi_0}(1 - e^{-u_p/\lambda}). \tag{44}$$

This quasistatic expression differs from Eq. (14) by the factor $1-\exp(-u_p/\lambda)]/2$, which accounts for the finite Meissner currents at the pin, $x = u_p$, and the fact that the trapped vortex does not go back as B_t changes sign, thus dissipating half of what is given by Eq. (14).

B. Residual surface resistance at $B_0 \ll B_v$

Besides dissipation due to vortex penetration and exit, there is also dissipation due to rf oscillations of vortices already trapped in the sample.[74] In this section we address rf dissipation and depinning of vortices trapped in a superconductor during field cooling, in the limit of very low flux density, for which the intervortex interaction is negligible.

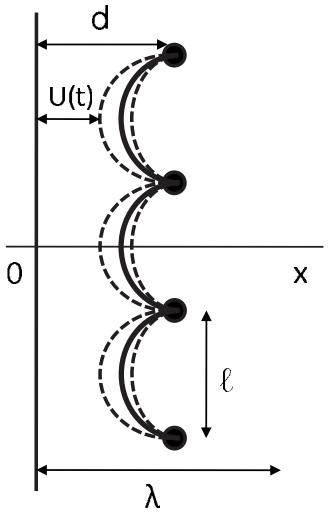

FIG. 13. Vortex pinned by a chain of defects near the surface. The solid line shows the equilibrium vortex shape due to competition of pinning and the image attraction forces. The dashed lines show instantaneous vortex profiles for $B(t)=B_0$ and $B(t)=-B_0$, between which the vortex line oscillates.

We first consider a single vortex pinned by a chain of equidistant defects spaced by ℓ from each other and by d from the surface in the layer of rf field penetration, as shown in Fig. 13. In this case the equation of motion of the vortex line takes the form

$$\eta_0 \dot{u} = \epsilon u'' + \frac{\phi_0 B_0}{\mu_0 \lambda} e^{-u/\lambda} \sin \omega t - \frac{\phi_0^2}{2\pi\mu_0 \lambda^3} K_1\left(\frac{2u}{\lambda}\right) + \sum_m f_p(u, y - m\ell), \tag{45}$$

where the first term on in the rhs describes the bending stress of the vortex line, the prime means differentiation over the coordinate y along the surface, and the last term is the sum of the elementary pinning forces $f_p(x,y)$. For $\ell > \lambda$, the dispersive vortex line tension ϵ reduces to the vortex self-energy $\epsilon = \phi_0 B_{c1}/\mu_0$ per unit length.[42]

As evident from Fig. 13, the magnetic attraction to the surface makes the pinned vortex not straight even at zero rf field. As a result, there is a minimum trapping distance d_m, so that only vortices spaced by $u > d_m$ can be pinned. Vortices spaced by $u < d_m$ are unstable and annihilate at the surface, since the image attraction prevails over pinning. For weak identical pins, d_m can be evaluated from the force balance equation

$$\frac{\phi_0^2}{2\pi\mu_0 \lambda^3} K_1\left(\frac{2d_m}{\lambda}\right) = \frac{f_p}{\ell}, \tag{46}$$

where f_p is the maximum pinning force per pin. The vortex segments between the pins bow out toward the surface, but for vortices in the trapped flux zone $x > d_m$, the curvature of $u(y)$ is weak and the image attraction force $F_i = (\phi_0^2/2\pi\mu_0\lambda^3) K_1(2u/\lambda)$ is nearly uniform. In this case the equilibrium shape of the vortex segment between the pins is determined by the equation $\epsilon u_0'' = F_i$ with $u_0(\pm \ell/2) = d$, which yields the parabolic profile

$$u_0(y) = d - u_{0m}\left(1 - \frac{4y^2}{\ell^2}\right), \tag{47}$$

$$u_{0m} = \frac{\phi_0^2 \ell^2}{16\pi\mu_0 \epsilon \lambda^3} K_1\left(\frac{2d_m}{\lambda}\right) = \frac{\ell^2 K_1(2d_m/\lambda)}{4\lambda \ln \tilde{\kappa}}. \tag{48}$$

Here $\epsilon = \phi_0^2(\ln \kappa + c_v)/4\pi\mu_0\lambda^2$ where the constant $c_v \approx 0.5$ accounts for the vortex core contribution. It is convenient to use the effective $\tilde{\kappa} \approx 1.65\kappa$ defined by $\ln \tilde{\kappa} = \ln \kappa + c_v$. Equations (47) and (48) correspond to $\ell \gg \lambda$, so the condition that $u_{0m} \ll \lambda$ is provided by $d_m > \lambda$, as follows from Eq. (46). For denser pins, $\ell < \lambda$, the nonlocal expression for ϵ should be used,[42] in which case $\ln \kappa$ in Eq. (48) is to be replaced by $\ln(\ell/\xi)$.

To calculate the power Q_v dissipated by the pinned vortex under the weak ($B_0 \ll B_v$) rf field, we seek a solution of Eq. (45) in the form $u(y,t) = u_0(y) + \delta u(y,t)$. Here the Fourier component $\delta u_\omega(y) = \int \delta u(y,t) e^{-i\omega t} dt$ of the oscillating vortex displacement $\delta u(y,t)$ satisfies the linearized equation

$$i\omega\eta_0 \delta u_\omega = \epsilon \delta u_\omega'' + f_\omega, \tag{49}$$

where $f_\omega = \phi_0 B_0 \exp(-d/\lambda)/\mu_0\lambda$. In Eq. (49) we neglect the image force $\propto \exp(-2d/\lambda)\delta u$, which is much smaller than the first elastic term on the rhs for weak pinning and $d > d_m$ defined by Eq. (46). The solution of Eq. (49) with the boundary condition of the fixed vortex ends at the pins, $\delta u_\omega(\pm \ell/2)$, has the form

$$\delta u_\omega = \frac{f_\omega}{i\omega\eta_0}\left(1 - \frac{\cos[(1-i)\Omega_p^{1/2} y/\ell]}{\cos[(1-i)\Omega_p^{1/2}/2]}\right), \tag{50}$$

$$\Omega_p = \omega\tau_p, \quad \tau_p = \eta_0 \ell^2/2\epsilon. \tag{51}$$

Here we introduced the pinning relaxation time constant τ_p and the dimensionless frequency Ω_p. The dissipated power per unit vortex length,

$$Q_v = \frac{\eta_0 \omega^2}{2\ell} \int_{-\ell/2}^{\ell/2} |\delta u_\omega(y)|^2 dy, \tag{52}$$

can be calculated substituting here, Eq. (50), and integrating over y:

$$Q_v = \frac{f_\omega^2}{2\eta_0} \Gamma_\omega(\sqrt{\Omega_p}), \tag{53}$$

$$\Gamma_\omega(z) = 1 - \frac{\sinh z + \sin z}{z(\cosh z + \cos z)}. \tag{54}$$

For $\omega\tau_p \gg 1$, Eq. (53) gives the frequency-independent limit $Q_{vm} \to f_\omega^2/2\eta_0$, inversely proportional to η_0. However, for $\omega\tau_p \ll 1$, we obtain the quadratic frequency dependence $Q_v = f_\omega^2 \eta_0 \ell^4 \omega^2/240\epsilon^2$ proportional to η_0.

The vortex rf power $Q_v/a = B_0^2 R_i/2\mu_0^2$ per unit surface area results in the additional surface resistance R_i:

$$R_i = \frac{\phi_0^2 \langle e^{-2d/\lambda} \rangle}{\lambda^2 \eta_0 a} \Gamma_\omega(\sqrt{\Omega_p}), \tag{55}$$

where a is a mean spacing between pinned vortices and $\langle \cdots \rangle$ means averaging over the vortex positions d in the direction perpendicular to the surface. Since these positions must satisfy the stability condition $d > d_m$, the main contribution to R_i comes from vortices in the critical belt $d_m < d < d_m + \lambda$ where $\langle e^{-2d/\lambda} \rangle$ is maximum. For $\omega \tau_p \ll 1$, Eq. (55) simplifies to

$$R_i = \frac{\pi \mu_0^2 \omega^2 \ell^4 \kappa^2 \langle e^{-2d/\lambda} \rangle}{15 a \rho_n \ln^2 \tilde{\kappa}}, \tag{56}$$

where we used the Bardeen-Stephen η_0 and took $\epsilon = \phi_0^2 \ln \tilde{\kappa}/4\pi\mu_0\lambda^2$ for $\ell > \lambda$ or $\ln \kappa \to \ln(\ell/\xi)$ for $\xi \ll \ell \ll \lambda$.[42] These results show the following.

(i) For $\omega \tau_p \ll 1$, the frequency dependence of R_i is similar to the BCS surface resistance $R_{BCS} \propto \omega^2 \exp(-\Delta/T)$ at $T \ll T_c$. However, unlike $R_{BCS}(T)$, the vortex contribution R_i remains finite at $T \to 0$, so trapped vortices can contribute to the non-BCS excess surface resistance, which has been often observed on many superconductors at low temperatures. In this case even a few pinned vortices can result in R_i comparable to the exponentially small $R_{BCS}(T)$. This scenario was first suggested by Rabinowitz[74] who modeled pinning by a phenomenological spring constant and did not consider the critical depinning spacing d_m due vortex attraction to the surface. The account of a more realistic discrete pin structure is given in Fig. 13, and the gradient of the Lorentz force changes the frequency dependence of R_i and results in new effects discussed below.

(ii) R_i increases significantly as the superconductor gets dirtier. To evaluate this effect, we make a rough estimate $\langle \exp(-2d/\lambda) \rangle \sim \exp(-2d_m/\lambda)\lambda/a$, which takes into account the main contribution to R_i from vortices in the critical belt $d_m < d < d_m + \lambda$. Taking $\exp(-2d_m/\lambda)$ from Eq. (46) and using the asymptotic expansion $K_1(z) = (\pi/2z)^{1/2} \exp(-z)$, we obtain

$$R_i \sim \frac{4\pi^2 \mu_0^3 \omega^2 \ell^3 \kappa^2 \lambda^4 f_p}{15 a^2 \phi_0^2 \rho_n \ln^2 \tilde{\kappa}} \sqrt{\frac{d_m}{\pi\lambda}}. \tag{57}$$

Equation (57) shows that $R_i \propto 1/a^2$ is proportional to the trapped flux density, similar to the Bardeen-Stephen flux flow resistivity. In the dirty limit, $\lambda \simeq \lambda_0(\xi_0/\ell_i)^{1/2}$, $\xi \simeq (\xi_0 \ell_i)^{1/2}$, and $\rho_n \propto 1/\ell_i$, we obtain that the excess resistance $R_i \propto \rho_n^3$ increases rapidly as the resistivity increases (here the slowly varying logarithmic dependences of R_i on ℓ_i are neglected). This behavior of R_i has been observed on Nb cavities in which the change of ρ_n at the surface was caused by a low-temperature baking.[75–77]

(iii) There is a strong dependence of R_i on the size ℓ of pinned vortex segments because shorter segments have stiffer spring constants $\sim \epsilon/\ell^2$ and thus smaller vibration amplitudes under a rf field. If pinning centers are distributed randomly, $R_i(\ell)$ should be therefore averaged over the distribution of the segment lengths:

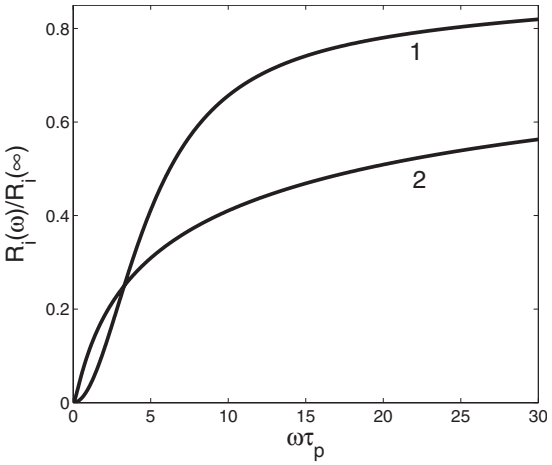

FIG. 14. Frequency dependences of the residual surface resistance due to pinned vortices. Curve 1 corresponds to R_i for a periodic chain of pins described by Eq. (55), and curve 2 corresponds to R_i for the exponential distribution of pinned vortex segments given by Eq. (59). Here $R_i(\infty) = \phi_0^2 \langle e^{-2d/\lambda} \rangle / \lambda^2 \eta_0 a$.

$$\bar{R}_i(\omega) = \int_0^\infty R_i(\omega \eta_0 \ell^2/2\epsilon) P(\ell) d\ell, \tag{58}$$

where R_i is given by Eq. (55) and $P(\ell)$ is a distribution function of the segment lengths. For example, $P(\ell)$ can be taken in the form $P(\ell) = \ell_0^{-1} \exp(-\ell/\ell_0)$ used in the Granato-Lücke model of pinned dislocations, where ℓ_0 is the mean segment length.[78] In this case, Eqs. (54), (55), and (58) yield

$$\bar{R}_i(\Omega_p) = \frac{R_\infty}{\sqrt{\Omega_p}} \int_0^\infty e^{-z\Omega_p^{-1/2}} \Gamma_\omega(z) dz, \tag{59}$$

where $z = \ell \Omega_p^{1/2}/\ell_0$, $\Omega_p = \omega \eta_0 \ell_0^2/2\epsilon$, and $R_\infty = \phi_0^2 \langle e^{-2d/\lambda} \rangle / \lambda^2 \eta a$ is the high-frequency limit of $R_i(\omega)$. The resulting behavior of $\bar{R}_i(\omega)$ is shown in Fig. 14: for low frequencies, the contribution of weakly pinned large-length segments makes $\bar{R}_i(\omega)$ higher than $R_i(\omega)$, while for high frequencies, the contribution of strongly pinned small segments makes $\bar{R}_i(\omega)$ lower than $R_i(\omega)$. The overall behavior of $\bar{R}_i(\omega)$ resembles the power-law dependence $R_i \propto \omega^\beta$ with $\beta \simeq 0.5–0.7$, which has been observed on Pb (Ref. 79) and Nb (Ref. 80) at 0.1–10 GHz.

To estimate the pinning time constant τ_p, we first evaluate the mean length of the vortex segment ℓ_0. This can be done from an estimate of the single-vortex pinning force balance $f_p \sim J_c \phi_0 \ell_0/\mu_0$, which expresses ℓ_0 in terms of the depinning critical current density J_c. For core pinning, $f_p \simeq \zeta B_c^2 \pi \xi^2/\mu_0$, where ζ accounts for the change in the condensation energy by the pin due to variation of $\delta T_c/T_c$ and the mean free path.[72] Hence,

$$\ell_0 \simeq \frac{\zeta \phi_0}{8\pi\mu_0 \lambda^2 J_c}. \tag{60}$$

Taking $\lambda = 40$ nm and $J_c = 10^9$ A/m^2 for Nb at $T \ll T_c$ yields $\ell_0 \sim 10^3 \zeta \lambda$. The pinning relaxation time τ_p can then be obtained from Eqs. (51) and (60):

$$\tau_p \simeq \frac{\zeta^2 \phi_0^2}{64\pi^2 \mu_0 \rho_n \lambda^2 \xi^2 J_c^2 \ln \tilde{\kappa}}. \quad (61)$$

Taking $\lambda \approx \xi \approx 40$ nm, $J_c = 10^9$ A/m^2, and $\rho_n = 10^{-9}$ Ω m for Nb, we obtain $\tau_p[s] \sim 210^{-6}\zeta^2$. From the rf measurements of pinning relaxation time $\sim 10^{-8}$ s in Nb,[80] we then deduce $\zeta \sim 0.1$ and $\ell_0 \sim 10^2\lambda \simeq 4$ μm. Here τ_p is rather sensitive to the value of ζ determined by details of the order parameter suppression at the pin.

It is instructive to compare Q from an oscillating vortex with Q due to the rf electric field $E_i \simeq B_0\omega\lambda \exp(-d/\lambda)$ induced in the fixed normal vortex core. In the latter case the power $Q_v \simeq \pi\xi^2 E_i^2/\rho_n$ gives the surface resistance $R_i \sim \pi\omega^2\lambda^4 \exp(-2d/\lambda)/\mu_0^2\kappa^2 a\rho_n$, which is by a factor of $\kappa^{-4}\ln^2\kappa \ll 1$ smaller than R_i given by Eq. (56) for an oscillating vortex segment. Thus, for type-II superconductors with $\kappa \gg 1$ considered in this paper, the inductive contribution[74] is negligible.

C. Low-field nonlinear surface resistance and rf annealing of trapped magnetic flux

So far we have considered R_i independent of the rf field. However, because R_i is mostly determined by pinned vortices in the critical belt $d_m < d < d_m + \lambda$, the excess resistance R_i may become dependent on the weak rf field due to an increase of the critical distance d_m as B_0 increases. This effect is evident from Fig. 13, which shows that, because both the image attraction force and the Meissner rf force increase as the vortex moves closer to the surface during the negative rf cycle, the vortex oscillations become asymmetric and shifted toward the surface. Thus, some of the pinned vortices can be pushed out of the sample by the rf field because d_m increases as B_0 increases.

To calculate the effect of the rf field on d_m, we consider the maximum depinning force due to the interaction between a vortex and the surface. This force, given by the sum of the second and third terms on the rhs of Eq. (45), contains the static image attraction force and the maximum instantaneous Lorentz force, which both push the vortex toward the surface during the negative rf cycle. Hence we obtain the following equation for d_m:

$$\frac{f_p}{\ell} = \frac{\phi_0^2}{2\pi\mu_0\lambda^3} K_1\left(\frac{2d_m}{\lambda}\right) + \frac{\phi_0 B_0}{\mu_0\lambda} e^{-d_m/\lambda}. \quad (62)$$

For weak pinning $\exp(-2d_m/\lambda) \ll 1$, we can use $K_1(z) \simeq (\pi/2z)^{1/2}\exp(-z)$ and reduce Eq. (62) to a quadratic equation for $\exp(-d_m/\lambda)$, which yields

$$e^{-2d_m/\lambda} = \frac{e^{-2d_{m0}/\lambda}}{[\sqrt{(B_0/B_\phi)^2 + 1} + B_0/B_\phi]^2}, \quad (63)$$

$$B_\phi = \left(\frac{\mu_0 f_p}{\lambda\ell}\right)^{1/2}\left(\frac{\lambda}{\pi d_m}\right)^{1/4}, \quad (64)$$

where the static d_{m0} is determined by Eq. (46). From Eqs. (63) and (56) we obtain the field dependence of R_i:

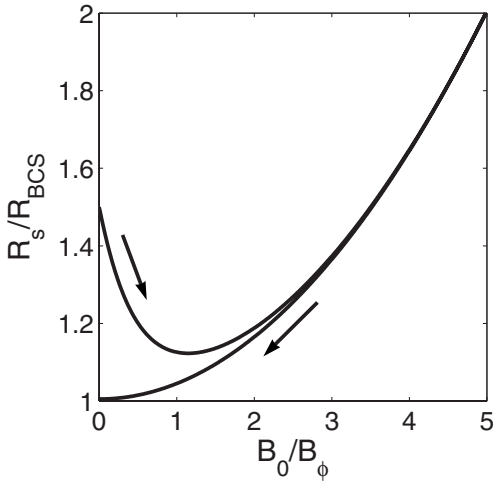

FIG. 15. The hysteretic field dependence of $R_s(B_0)$ defined by Eq. (66) for $\gamma = 1$, $B_\phi = 0.2B_c$, and $R_i(0) = 0.5R_{BCS}$. The descending branch is determined by Eq. (66) in which B_0 in the last term stays at the maximum $B_0 = 5B_\phi$ reached on the ascending branch.

$$R_i(B_0) = \frac{R_i(0)}{[B_0/B_\phi + \sqrt{1 + (B_0/B_\phi)^2}]^2}, \quad (65)$$

where the zero-field $R_i(0)$ is given by Eq. (56). For core pinning $f_p \sim \epsilon \sim \phi_0^2/4\pi\mu_0\lambda^2$, the crossover field $B_\phi \sim B_{c1}\sqrt{\lambda/\ell}$ can be much smaller than B_c. At low fields $B_0 \ll B_\phi$, the resistance $R_i(B_0) \simeq (1 - 2B_0/B_\phi)$ decreases linearly as B_0 decreases, while for high fields $B_0 \gg B_\phi$, Eq. (65) yields $R_i(B_0) \simeq R_i(0)B_\phi^2/4B_0^2$.

The decrease of $R_i(B_0)$ results from the field-induced shift of the critical belt $d_m < d < d_m + \lambda$ away from the surface, where the screening of the rf Meissner currents reduces vortex dissipation. As a result, the rf field irreversibly pumps parallel vortices out of a superconductor, resulting in a rf "annealing" of the field-cooled trapped magnetic flux. The field dependence of $R_i(B_0)$ is therefore hysteretic: if B_0 is first increased to a maximum value B_{0m} and then decreased back to zero, $R_i(B)$ on the ascending branch decreases according to Eq. (65) and stays equal to $R_i(B_{0m})$ on the descending branch as shown in Fig. 15. This hysteretic behavior enables an experimental separation of the vortex contribution to R_i from reversible mechanisms due to sound generation,[81] dielectric losses in the substrate,[82,83] etc.

The total surface resistance R_s can be written as a sum of the vortex component R_i and the BCS resistance:

$$R_s = R_{BCS}\left[1 + \gamma\frac{B_0^2}{B_c^2}\right] + \frac{R_i(0)}{[B_0/B_\phi + \sqrt{1 + B_0^2/B_\phi^2}]^2}. \quad (66)$$

Here we included the first nonlinear field correction to R_{BCS} due to the Doppler shift of the quasiparticle spectrum and heating effects. In the clean limit the Doppler contribution $\gamma_p \sim (\Delta/T)^2$ increases as T decreases,[87–91] while the heating component $\gamma_h \propto R_{BCS}$ decreases as T decreases.[91] The total $R_s(B_0)$ exhibits a nonmonotonic field dependence: $R_s(B_0)$ first *decreases* as B_0 increases, reaching the minimum at B_0

$=B_{min}$, and then increases at $B_0>B_{min}$, as shown in Fig. 15. Here B_{min} can be found from Eq. (66):

$$B_{min} \simeq \sqrt{B_c B_\phi}\left(\frac{R_i(0)}{4\gamma R_{BCS}}\right)^{1/4}, \quad B_{min} \gg B_\phi, \tag{67}$$

$$B_{min} \simeq \frac{B_c^2 R_i(0)}{\gamma B_\phi R_{BCS}}, \quad B_{min} \ll B_\phi. \tag{68}$$

As illustrated by Fig. 15, the rf field cycling could reduce the surface resistance by irreversibly pumping a fraction of trapped flux out of the sample. The rf flux annealing considered in this paper is somewhat analogous to a directional motion of magnetic flux induced by transport ac current, resulting in a dc voltage on a superconductor.[84–86]

V. NONLINEAR HOT SPOTS IN THE SURFACE RESISTANCE

Localized dissipation due to vortex penetration or oscillation of pinned vortices in thick films produces a long-range temperature distribution, which spreads out on the scale $\sim 2d/\pi$, much greater than λ (see Fig. 8). Even if these temperature variations are weak, $\delta T(\mathbf{r})=T(\mathbf{r})-T_0 \ll T_0$, they can nevertheless produce strong variations in the surface resistance R_s of the surrounding areas, resulting in nonlinear contributions to R_s with very different field and frequency dependences than $R_{BCS}(T,\omega)$. This effect comes from the exponential temperature dependence of the BCS surface resistance,

$$R_{BCS}(\mathbf{r}) \propto \frac{\omega^2}{T}\exp\left[-\frac{\Delta}{T_0}+\frac{\delta T(\mathbf{r})\Delta}{T_0^2}\right], \tag{69}$$

so that even weak variations $\delta T(\mathbf{r})<T_0$ can produce strong variations in $R_{BCS}(\mathbf{r})$ at low temperatures $T_0^2<\delta T\Delta$. Indeed, substituting the surface temperature distribution $\delta T(0,y)=(Q/\pi k)\ln\coth(\pi y/4d)$ from Eq. (30) at $x=0$ into Eq. (69) we obtain

$$R_s(y)=R_{BCS}(T_0,\omega)\coth^\sigma\left(\frac{\pi y}{4d}\right), \tag{70}$$

$$\sigma(B_0,T_0,\omega)=Q(B_0,T_0,\omega)\Delta(T_0)/\pi k(T_0)T_0^2, \tag{71}$$

on the scales $|y|>r_0$ greater than the size r_0 of the heat source. Here the exponent σ is proportional to the dissipated power Q, which depends on both B_0 and ω. For example, $Q\propto(B_0^2-B_v^2)^{\omega\tau_2}$ near the onset of the single-vortex penetration [see Eq. (15)] or $Q\propto B_0^2\Gamma_\omega(\Omega_p)$ for a pinned vortex near the surface [see Eq. (53)]. In turn, the dependences of σ on B_0 and ω result in a nonlinear contribution to the global surface resistance from sparse "hot spots" of size of the film thickness around much smaller heat sources.[91] These hot spots contributions can have very different dependencies on B_0 and ω as compared to the field-independent $R_{BCS}\propto\omega^2$. For $\sigma<1$, the total excess resistance $\delta\Re_s$ is insensitive to the power distribution $q(x)$ and can be obtained by integrating Eq. (70) using a new variable $\varphi=\tanh^2(\pi y/4d)$:

$$\delta\Re_s=\int_{-\infty}^{\infty}[R_s(y)-R_{BCS}]dy=\frac{4d}{\pi}\left[\psi\left(\frac{1}{2}\right)-\psi\left(\frac{1-\sigma}{2}\right)\right]R_{BCS}, \tag{72}$$

where $\psi(x)=d\ln\Gamma(x)/dx$ and $\Gamma(x)$ is the gamma function.[57] For $\sigma\ll 1$, the expression in the brackets reduces to $\pi^2\sigma/4$; thus,

$$\delta\Re_s=\pi d\sigma(B_0,\omega,T_0)R_{BCS}, \quad \sigma\ll 1. \tag{73}$$

If Q is due to pinned vortices, the correction $\delta\Re_s$ from weak hot spots with $\sigma\ll 1$ is quadratic in B_0 and proportional to ω^4 for low frequencies $\omega\tau_p\ll 1$ [see Eq. (56)]. As $\sigma\to 1$, the function in the brackets in Eq. (72) diverges logarithmically, indicating that the spatial distribution of the power density $q(x)$, which cuts off the logarithmic divergence in $T(x,y)$ in Eqs. (29), should be taken into account.

In the crossover region $\sigma\sim 1$, the behavior of $\delta\Re(B_0,\omega)$ is sensitive to the details of the power density distribution $q(x)$, but in the limiting case $\sigma\gg 1$ the main contribution to $\delta\Re$ comes from the hottest region near the heat source for which $\delta T(y)$ is given by Eq. (31). Substituting Eq. (31) into Eq. (69), we obtain

$$\frac{\delta\Re_s}{R_{BCS}}\simeq\int_{-\infty}^{\infty}dy\left[\frac{16d^2}{\pi^2(y^2+r_0^2)}\right]^{\sigma/2}=r_0\left(\frac{4d}{\pi r_0}\right)^\sigma I_\sigma, \tag{74}$$

where $I_\sigma=\sqrt{\pi}\Gamma[(\sigma-1)/2]/\Gamma(\sigma/2)\approx(2\pi/\sigma)^{1/2}$ for $\sigma\gg 1$. The behavior of $\delta\Re_s$ for $\sigma>1$ changes radically as compared to $\sigma<1$: instead of relatively weak power-law dependences of $\delta\Re_s$ on B_0 and ω for $\sigma<1$, Eq. (74) predicts much stronger exponential field and frequency dependences of $\delta\Re_s$ for $\sigma>1$, $r_0\ll d$. The case of strong dissipation $\sigma>1$ can result from vortex penetration amplified by grain boundaries,[92,93] surface topography,[4] local enhancements of R_{BCS} due to impurity segregation, etc.

The mean surface resistance $\bar{R}_s$ averaged over all hot spot contributions is given by

$$\bar{R}_s=R_{BCS}+\bar{R}_i+\sum_n\delta\Re_s(\mathbf{r}_n)/A. \tag{75}$$

Here the averaged residual resistance $\bar{R}_i$ results from either pinned vortices or other mechanisms, the last term on the rhs is due to the effect of vortex dissipation on the BCS resistance, $\mathbf{r_n}$ are the coordinates of the sparse (thermally noninteracting) hot spots, and A is the surface area exposed to the rf field. As shown above, $\delta\Re_s$ can have very different temperature and frequency dependences as compared to R_{BCS}, so the hot spot contribution can strongly affect the dependences of the global surface resistance $\bar{R}_s$ of ω and T, particularly at low temperatures, where R_{BCS} is exponentially small. Moreover, the last two terms on the rhs of Eq. (75) can bring about a strong dependence of $\bar{R}_s$ on the rf amplitude, which can be well below the field $\sim B_cT/T_c$ of intrinsic nonlinearities of the BCS surface resistance due to the Doppler shift of quasiparticle energies.[87–91]

Thermal instabilities ignited by hot spots

In the previous section we considered the rf power as a function of the bath temperature T_0. However, Q is actually determined by the local temperature T_m, which should be calculated self-consistently from the heat balance condition. We consider the case for which the mean spacing between hot spots, L_i, is shorter than the thermal length $L_\theta = (dk/\alpha_\theta)^{1/2}$, over which $\delta T(\mathbf{r})$ decays away from a single hot spot. Here $\alpha_\theta = k\alpha_K/(d\alpha_K + k)$ is the effective thermal resistance across the film which accounts for the resistance d/k due to thermal conductivity plus the interface thermal resistance $1/\alpha_K$, where α_K is the Kapitza heat transfer coefficient. For $L_i \ll L_\theta$, thermal fields of hot spots overlap and the temperature T_m along the surface becomes uniform. In this case the thermal balance equation takes the form

$$(T_m - T_0)\alpha_\theta = \frac{B_0^2}{2\mu_0^2}[R_i + R_{BCS}(T_m)], \tag{76}$$

which determines self-consistently both the rf dissipated power and the maximum temperature T_m as functions of B_0 and ω. It is convenient to express $B_0(T_m)$ as a function of T_m from Eq. (76):

$$B_0^2 = \frac{2\mu_0^2(T_m - T_0)\alpha_\theta}{R_i + R_0 \exp[(T_m - T_0)\Delta/T_0^2]}. \tag{77}$$

Here we took into account the most essential exponential temperature dependence of the BCS surface resistance, where $R_0 = R_{BCS}(T_0)$, and the residual resistance R_i due to trapped vortices is assumed temperature independent for $T \ll T_c$. The function $B_0(T_m)$ has a maximum at

$$T_m - T_0 = \frac{T_0^2}{\Delta} + \frac{B_0^2 R_i}{2\mu_0^2 \alpha_\theta}, \tag{78}$$

giving the critical overheating $T_m - T_0 \ll T_0$ above which a thermal instability develops. From Eqs. (78) and (77), we obtain the equation for the maximum field B_p:

$$\frac{R_0 B_p^2 e\Delta}{2\mu_0^2 T_0^2 \alpha_\theta} \exp\left(\frac{R_i B_p^2 \Delta}{2\mu_0^2 T_0^2 \alpha_\theta}\right) = 1. \tag{79}$$

The thermal balance equation (76) has solutions $T_m(B_0)$ only if the rf amplitude is below the breakdown field B_p. For $B_0 > B_p$, the thermal runaway occurs because the heat generation grows faster than the heat flux to the coolant as T_m increases. This situation is analogous to combustion in chemical systems[94] or thermal quench in semiconductors, normal metals, or superconductors.[34]

For $R_i \ll R_0$, the exponential term in Eq. (79) can be neglected and the breakdown field is given by[91]

$$B_p = \mu_0\left(\frac{2\alpha_\theta T_0^2}{R_0 e\Delta}\right)^{1/2}. \tag{80}$$

The temperature dependence of $B_p(T_0)$ can be obtained taking $R_0(T_0) = R_{n0}(\Delta/T_0)\exp(-\Delta/T_0)$ and $\alpha_\theta = \alpha' T_0^s$, from which $B_p(T_0) \propto T_0^{(3+s)/2} \exp(-\Delta/2T_0)$ reaches a minimum at $T_{min} = \Delta/(s+3)$ and increases as T_0 decreases below T_{min}. However, for lower temperatures, $R_{BCS}(T_0)$ becomes smaller than R_i in which case the exponential term in Eq. (79) dominates and $B_p(T_0) \sim \mu_0(2\alpha_\theta T_0^2/R_i\Delta)^{1/2} \propto T_0^{1+s/2}$ decreases as T_0 decreases. The behavior of $B_p(T_0)$ is shown in Fig. 16. The maximum in $B_p(T)$ at the optimum temperature T_{max} separates the regimes controlled by the BCS surface resistance at $T_0 > T_{max}$ and by hot spots due to frozen flux or other mechanisms of residual resistance at $T_0 < T_{min}$. For Nb ($\Delta \approx 18$ K), the optimum temperature in Fig. 16 corresponds to $T_{max} \simeq 2$ K, while for Nb_3Sn ($\Delta \approx 36$ K), $T_{max} \simeq 4$ K, if R_i/R_{n0} is the same for both materials. The above consideration based on the linear BCS surface resistance assumes that the breakdown field B_p is much smaller than the field $\simeq TB_c/T_c$ at which the intrinsic nonlinearities in R_s become important. A significant increase of the isothermal $R_s(B_0)$ due to these nonlinearities can strongly affect the thermal breakdown,[91] limiting B_p by the thermodynamic critical field B_c.

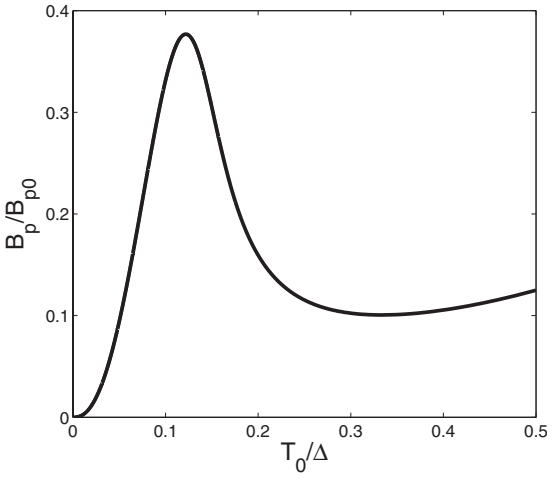

FIG. 16. The temperature dependence of $B_p(T_0)$ calculated from Eq. (79) for $R_{BCS}(T_0) = R_{n0}(\Delta/T_0)\exp(-\Delta/T_0)$, $R_i/eR_{n0} = 2\times10^{-5}$, $\alpha_\theta = \alpha' T_0^s$, $s=3$, and $B_{p0}^2 = 2\mu_0^2\alpha' T_0^{s+1}/R_{n0}$.

VI. DISCUSSION

The results presented above show that the breakdown of the Meissner state by strong rf fields involves supersonic vortex penetration through the surface barrier weakened by defects, the jumpwise LO-type instability, and high dissipation even for single vortices. Such dissipation results in thermal retardation effects and hot spots igniting the explosive thermal instability due to the exponential temperature dependence of the surface resistance. These effects are precursors of the avalanche vortex penetration and dendritic thermomagnetic instabilities.[64,65]

At the onset of vortex penetration pinning forces are much weaker than the driving forces of the rf Meissner currents. Yet as the vortex moves away from the surface by the distance $\sim\lambda$, the Lorentz force decreases exponentially, so the vortex can be trapped by pinning centers. Such vortices trapped in the thin surface layer of rf field penetration during breaking through the surface barrier or field cooling of the sample can result in a temperature-independent residual surface resistance. Because pinning centers are distributed ran-

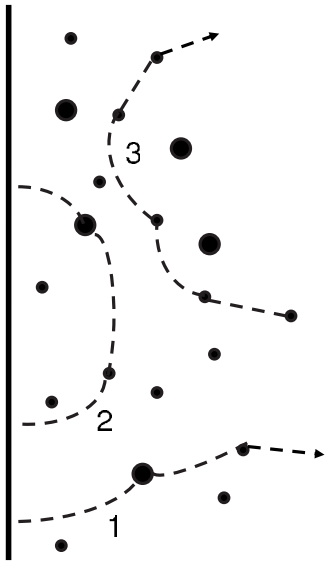

FIG. 17. Vortices (shown as dashed lines) trapped near the surface by pinning centers (black dots).

domly, the rf power dissipated by pinned vortices $Q(u)$ varies very strongly because of the exponential sensitivity of $Q \propto \exp(-2u/\lambda)$ to the vortex position. This effect results in hot spots of vortex dissipation, which peaks for vortices spaced from the surface by distances close to the minimum distance d_m, for which pinning forces can prevent vortex annihilation at the surface at low fields $B_0 \ll B_v$. The field dependence of d_m causes rf flux annealing in which vortices are irreversibly pushed out from the surface layer. This effect results in a nonlinear hysteretic dependence of $R_i(B)$ at low fields $B_0 \ll B_c$, which may pertain to the puzzling decrease of the surface resistance at low fields $B_0 \sim 3-20$ mT, which has been often observed on Nb (Refs. 4 and 76) and other superconductors.[82,83] Yet Eq. (65) describes well the observed field dependence $R_i \propto 1/B_0^2$ for Nb.[76]

Besides the field and frequency dependences of $R_i(B)$, another manifestation of the vortex pinning mechanism is the hysteretic behavior shown in Fig. 15 due to the rf annealing of the trapped flux. This mechanism caused by the gradient of the Lorentz force is only effective for vortex segments parallel to the surface and does not affect vortex segments perpendicular to the surface. The segments of pinned vortices perpendicular to the surface generally give a field-independent contribution to R_i; however, if these segments belong to the vortex semiloop trapped at the surface, the rf Lorentz force gradient acting on the parallel component of the loop can eventually push the whole loop toward the surface where it shrinks and annihilates. In this case the rf annealing decreases R_s, eliminating some of the hot spots caused by trapped vortices. This is illustrated by Fig. 17, which shows three different types of vortices trapped at the surface. Vortex 1 cannot be pushed out by the rf field because only a small segment of it, $\sim\lambda$, is exposed to the rf Lorentz force, while the remaining part is pinned in the bulk. Vortex semiloop 2 can be pushed out by the rf field, as discussed above. Vortex 3 has a parallel segment, which, however, cannot annihilate at the surface because it is held back by other pinned segments which are beyond the surface layer of the rf field penetration.

Penetration and trapping of even single vortices at low temperatures can significantly increase the exponentially small R_s, which, in turn, decreases the thermal breakdown field B_p. For example, flux trapped during field cooling in the Earth magnetic field $B_i \simeq 40$ μT corresponds to the mean intervortex spacing $a=(\phi_0/B_i)^{1/2} \simeq 7$ μm. To estimate R_i for such trapped flux, we use Eq. (55) for strong pinning at $\omega\tau_p < 1$, taking $\langle \exp(-2d/\lambda) \rangle \sim \lambda/a$ and $d_m \sim \lambda$. Hence,

$$R_i \simeq \frac{\omega^2 \tau_p^2}{30} R_i(\infty), \quad R_i(\infty) = \frac{\rho_n B_i}{\lambda B_{c2}}, \tag{81}$$

where $R_i(\infty)$ is the high-frequency limit of $R_i(\omega)$. For Nb, taking $B_{c2}=400$ mT, $\lambda=40$ nm, $\rho_n=10^{-9}\Omega$ m, and $B_i=40$ μT, we obtain $R_i(\infty)=2.5$ $\mu\Omega$, much higher than the typical values $R_i \sim 10$ nΩ observed on high-purity Nb.[76] For Nb_3Sn, with $\rho_n=0.2$ $\mu\Omega$ m, $\lambda \simeq 90$ nm, we obtain $R_i(\infty) \simeq 3.9$ $\mu\Omega$. As follows from Eq. (81), pinning reduces R_i by the factor $(\omega\tau_p)^2/30$, so $R_i \simeq 10$ nΩ corresponds to $(\omega\tau_p)^2 \sim 0.1$, or $\tau_p \simeq 0.5$ ns for $\omega/2\pi=1$ GHz. By contrast, the pinning time constant $\tau_p \sim 10^{-8}$ s measured by Pioszyk *et al.*[80] seems to indicate that their Nb sample was in the weak pinning limit $(\omega\tau_p)^2 \gg 1$, for which $R_i \simeq R_i(\infty)$ is in agreement with the measured $R_i(0.5\ \text{Oe}) \simeq 2$ $\mu\Omega$ and the estimate from Eq. (81).

Introducing dense pinning structures in the surface layer of the rf field penetration can therefore impede vortex oscillations and significantly reduce the part of R_i caused by trapped flux, particularly for vortex loops like 1 and 3 in Fig. 17 which are not affected by the rf flux annealing. Because pinning is only effective if $\omega\tau_p < 1$, decreasing τ_p in Eq. (51) implies reducing the pin spacing. At the same time, a more effective rf flux annealing requires both weak and dense pins [small f_p and ℓ in Eq. (57)]. Overall, R_i can be reduced by decreasing the relaxation time constant τ_p, which can be done not only by decreasing the pin spacing ℓ, but also by optimizing the mean free path at the surface. Indeed, Eq. (51) shows that τ_p is larger for higher-κ superconductors because of the softening of the vortex line tension ϵ, although this effect can be offset by a higher normal resistivity. For example, the ratio $\tau_{p1}/\tau_{p2}=\kappa_1^2\rho_{n2}/\kappa_2^2\rho_{n1} \propto \rho_{n1}/\rho_{n2}$ for two different materials 1 and 2 (or two different mean free paths ℓ_i), but the same ℓ, shows that pinning becomes less effective for a dirtier surface. Furthermore, comparing Nb with $\kappa_1=1$, $\rho_{n1}=10^{-9}$ Ω m and Nb_3Sn with $\kappa_2=30$, $\rho_{n1}=0.2$ $\mu\Omega$ m, we obtain $\tau_p^{Nb}/\tau_p^{Nb_3Sn} \sim 1/5$. Thus, reduction of R_i by pinning turns out to be somewhat more effective in Nb, although this conclusion can be strongly affected by impurities, as discussed above.

The results of this work show that reducing vortex dissipation is an important problem in achieving ultimate pair-breaking breakdown fields in superconductors. In particular, significant progress has been made in increasing R_s and B_p by low-temperature annealing of Nb cavities which enables tuning the impurity concentration, nanoscale oxide layers, and hot spot distribution on the Nb surface.[76,77,95,96] Another possibility in raising the ultimate breakdown fields is to use

thin-film superconductor-insulator-superconducting (SIS) multilayer coating with high-B_c films of thickness $d<\lambda$ to significantly increase B_{c1} and delay the field onset of vortex penetration.[97] Moreover, the SIS coating may suppress the LO instability by decreasing the vortex flight time through the film and providing strong pinning due to the magnetic interaction of the vortex with the film surfaces. The SIS multilayer coating of Nb cavities may enable increasing the ultimate breakdown fields B_p above B_c^{Nb} by taking advantage of $A15$ superconductors[98] or MgB_2 (Refs. 99 and 100) with $B_c > B_c^{\mathrm{Nb}}$ and potentially lower R_{BCS}.

ACKNOWLEDGMENTS

The work at NHMFL is supported by NSF Grant No. DMR-0084173 with support from the state of Florida. The work at the Jefferson Laboratory is supported by the Jefferson Science Associates, LLC, under DOE Contract No. DE-AC05-060R23177.

APPENDIX A: TEMPERATURE OF A MOVING VORTEX

Equation (25) can be written in the dimensionless form

$$\dot{\theta} = \nabla^2\theta - \theta + \beta(\theta_m)s^2(t)f[x-u(t),y], \tag{A1}$$

where $\theta=(T-T_0)/(T_c-T_0)$ and the time, coordinates, and vortex velocity are normalized by the thermal scales $t_\theta = C/\alpha$, $L_\theta=(k/\alpha)^{1/2}$, and $v_\theta=L_\theta/t_\theta$, respectively, $\beta(\theta_m) = \eta_0(\theta_m)v_\theta^2/(T_c-T_0)k$, and $s(t)=v/v_\theta$ is the dimensionless vortex velocity. The Fourier transform of Eq. (A1) results in the following equation for the Fourier components, $\theta_p(t) = \int \theta(x,y,t)\exp(-i\mathbf{pr})d^2\mathbf{r}$:

$$\dot{\theta}_{\mathbf{p}} + (1+p^2)\theta_{\mathbf{p}} = f_{\mathbf{p}}g(t)e^{-ip_x u(t)}, \tag{A2}$$

where $g(t)=\beta[\theta_m(t)]s^2(t)$. The solution of Eq. (A3) is

$$\theta_{\mathbf{p}}(t) = f_{\mathbf{p}}\int_0^\infty e^{-(1+p^2)t' - ip_x u(t-t')}g(t-t')dt'. \tag{A3}$$

For steady-state vortex oscillations, the rf field was turned on at $t_i=-\infty$ and $v(t)$ in Eq. (A3) accounts for all oscillations preceding the time t. For $f(r)=\pi^{-1}\xi_1^{-2}\exp(-r^2/\xi_1^2)$ and $f_{\mathbf{p}} = \exp(-p^2\xi_1^2/4)$, the inverse Fourier transform of Eq. (A3) gives

$$\theta(\mathbf{r},t) = \frac{1}{\pi}\int_0^\infty \frac{dt'g(t-t')}{4t'+\tilde{\xi}^2}e^{-t' - \{[x-u(t-t')]^2+y^2\}/(\tilde{\xi}^2+4t')}. \tag{A4}$$

Equation (A4) was obtained for an infinite sample. For a thermally insulated or ideally cooled surface at $x=0$, Eq. (A4) can be modified using the method of images:

$$\theta(\mathbf{r},t) = \frac{1}{\pi}\int_0^\infty \frac{dt'g(t-t')}{4t'+\tilde{\xi}^2}e^{-t'-y^2/(\tilde{\xi}^2+4t')} \times[e^{-[x-u(t-t')]^2/(\tilde{\xi}^2+4t')} \pm e^{-[x+u(t-t')]^2/(\tilde{\xi}^2+4t')}], \tag{A5}$$

where the plus and minus signs in the parentheses correspond to the Dirichlet $[\partial_x\theta(0,y,t)=0]$ and Neumann $[\theta(0,x,t)=0]$ boundary conditions at the surface, respectively. The core size is typically much smaller than L_θ, so the dynamic equation for the core temperature $\theta_m(t)$ can be obtained from the self-consistency condition $\theta_m(t) = \theta(u(t),0,t)$, resulting in Eq. (26).

Next we consider the steady-state temperature distribution $T(x,y)$ averaged over high-frequency vortex oscillations at $2\pi\omega t_\theta \gg 1$. In this case $T(x,y)$ satisfies the static thermal diffusion equation

$$k\nabla^2 T + q(x)\delta(y) = 0, \tag{A6}$$

where $q(x)$ is the mean power density distribution along the vortex trajectory. We solve Eq. (A6) for a film of thickness d with the boundary conditions $\partial_x T(x,y)=0$ on the thermally insulated surface $x=0$ where vortex dissipation is localized and $T(x,y)=T_0$ at the opposite surface, $x=d$ kept at T_0. By symmetry, this geometry has the same $T(\mathbf{r})$ as in a film of thickness $2d$ with isothermal boundary conditions $T(\pm d,y)=T_0$ and the heat source in the middle at $x\approx 0$. In this case Eq. (A6) can be solved using the Green function

$$G(\mathbf{r},\mathbf{r}') = \frac{1}{4\pi k}\ln\frac{\cosh\frac{\pi(y-y')}{2d} + \cos\frac{\pi(x+x')}{2d}}{\cosh\frac{\pi(y-y')}{2d} - \cos\frac{\pi(x-x')}{2d}}, \tag{A7}$$

which gives the distribution of $\delta T(\mathbf{r})=T(\mathbf{r})-T_0$:

$$\delta T(\mathbf{r}) = \frac{1}{2\pi k}\int_0^d q(x')\ln\frac{\cosh\frac{\pi y}{2d} + \cos\frac{\pi(x+x')}{2d}}{\cosh\frac{\pi y}{2d} - \cos\frac{\pi(x-x')}{2d}}dx'. \tag{A8}$$

If the length of the dissipation source $\sim r_0$ is much smaller than the film thickness, $\delta T(\mathbf{r})$ around the source at $(x^2,y^2) \ll d^2$ reduces to

$$\delta T(\mathbf{r}) = \frac{1}{2\pi k}\int_0^\infty q(x')\ln\frac{16d^2}{\pi^2[y^2+(x-x')^2]}dx'. \tag{A9}$$

Next, we take a rectangular approximation $q(x)=q_0$ for $x<r_0$ and $q(x)=0$ for $x>r_0$, where r_0 is a characteristic size of the dissipation source, so that $q_0 r_0 = Q$ gives the total power Q. In this case the distribution of $\delta T(0,y)$ along the surface becomes

$$\delta T(y) = \frac{q_0}{2\pi k}\int_0^{r_0}\ln\frac{16d^2}{\pi^2(y^2+x'^2)}dx', \tag{A10}$$

which yields after integration

$$\delta T(y) = \frac{Q}{2\pi k}\left[\ln\frac{16d^2}{\pi^2(y^2+r_0^2)} + 2 - \frac{2y}{r_0}\tan^{-1}\frac{r_0}{y}\right]. \tag{A11}$$

The maximum $\delta T_m = \delta T(0,0)$ is given by

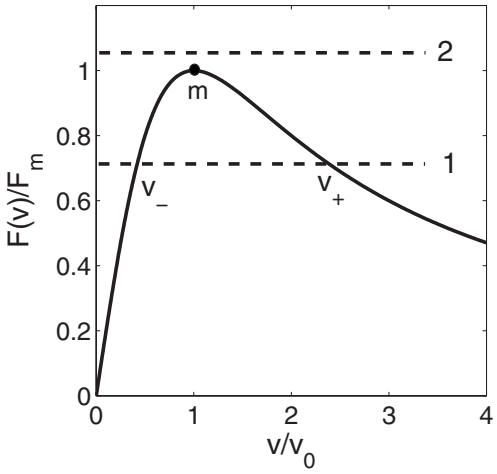

FIG. 18. Graphic solution of the equation $F(v)=F$, where $F(v)=\eta_0 v/(1+v^2/v_0^2)$. The branches $v_\pm$ correspond to the $\pm$ signs in Eq. (35), and the dashed lines show the Lorentz force F for particular values of u in the stable region (1) and the unstable region (2).

$$\delta T_m = \frac{Q}{\pi k}\left(\ln\frac{4d}{\pi r_0}+1\right). \tag{A12}$$

APPENDIX B: MULTIVALUED FRICTION FORCE

Equation (33) describes an overdamped vortex driven by the force $F(u,t)$ balanced by a nonlinear friction force $\eta v/(1+v^2/v_0^2)$. The force balance equation has either two or no roots, as shown in Fig. 18. The velocity $v_-(F)$ for the left intersection point vanishes at $F=0$ and increases up to v_0 as F increases. The velocity for the right intersection point $v_+(F)$ decreases as F increases. If $F<F_m$, the branch $v_-(F)$ describes all smooth parts of the vortex trajectory and also provides $v_-(0)=0$ for the initial condition $u(0)=0$. For $F>F_m$, the vortex jumps from $x=u_1$ to the point $x=u_2$ where friction is able to balance the drive. Here $u_{1,2}$ are defined by the condition $F(u_{1,2},t_{1,2})=F_m$. The branch $v_-(F)$ describes all smooth parts of $u(t)$ provided that $\dot{F}(u_{1,2},t)<0$, so that $F(t)$ always decreases below F_m after the jump.

For high rf frequencies or strong vortex core overheating, there are situations for which $\dot{F}>0$ after the jump. For example, if $u>\lambda$, the term with the $K(x)$ in F can be neglected and $\dot{F}=v_0\partial_x F+\partial_t F$ becomes

$$\dot{F} = (-v_0/\lambda + \omega\cot\omega t)F, \tag{B1}$$

which tends to become positive at higher frequencies. In this case the vortex cannot jump to the point where $F(u,t)=F_m$, since the friction force cannot balance F if $\dot{F}>0$, because $F(u,t)$ keeps increasing above F_m, so $v(t)$ becomes greater than v_0. Thus, for $\dot{F}>0$, friction can only stop the vortex jump if $v>v_0$; thus, we have to consider the branch $v_+(F)$ as well. We should therefore construct the trajectory for which the vortex first jumps at $t=t_i$ to the new point $x=u_i$ and acquires the velocity $v_i>v_0$. After that $v(t)$ continuously decreases from $v_i>v_0$ at $t=t_i$ to v_0 at $t=t_0$, as described by the first-order differential equation $\dot{u}=v_+[F(u,t)]$. Here u_0 and t_0 are determined by the equations

$$F[u_0,t_0]=F_m, \quad v_0\partial_u F+\partial_t F=0, \tag{B2}$$

which state that $\dot{F}$ should change sign as the vortex reaches the maximum friction force at the critical velocity $v-0$. Indeed, if $\dot{F}$ changes sign at any point of the descending branch $v_+(F)$, the vortex cannot reach v_0, so $v(t)$ passes through a minimum at some $v>v_0$ and then starts accelerating continuously. On the other hand, if the vortex reaches v_0 at $\dot{F}>0$, the jump instability occurs. Therefore Eq. (B2) provides the only way for a stable switch from the descending branch of $v_+(F)$ for $t_i<t<t_0$ to the ascending branch of $v_-(F)$. Once t_0 and u_0 are found from Eq. (B2), the coordinate of the jump, u_i, can be calculated for the vortex going backward in time, taking the initial condition $u=u_0$ and $F=F_m$, and then solving the equation $\dot{u}=v_+[F(t_0-\tilde{t})]$ with the "negative time" $\tilde{t}=t_0-t_i$, from $\tilde{t}=0$ to $\tilde{t}=t_0-t_i$.

[1] J. Bardeen, Rev. Mod. Phys. **34**, 667 (1962).
[2] N. B. Kopnin, Rep. Prog. Phys. **65**, 1633 (2002); *Theory of Nonequilibrium Superconductivity* (Clarendon Press, Oxford, 2001).
[3] F. Furuta, K. Saitoa, T. Saekia, H. Inouea, Y. Morozumia, T. Higoa, Y. Higashia, H. Matsumotoa, S. Kazakova, H. Yamaokaa, K. Uenoa, Y. Kobayashia, R. S. Orra, and J. Sekutowicz, in *Proceedings of the 2006 European Particle Accelerator Conference, Edinburgh, Scotland, 2006*, edited by C. Biscari, H. Owen, Ch. Petit-Jean-Genaz, J. Poole, and J. Thomason (CCLRC, Edinburgh, 2006).
[4] H. Padamsee, Supercond. Sci. Technol. **14**, R28 (2001); IEEE Trans. Appl. Supercond. **15**, 2432 (2005).
[5] P. J. Hirschfeld, W. O. Putikka, and D. J. Scalapino, Phys. Rev. Lett. **71**, 3705 (1993); Phys. Rev. B **50**, 10250 (1994).
[6] A. J. Berlinsky, D. A. Bonn, R. Harris, and C. Kallin, Phys. Rev. B **61**, 9088 (2000).
[7] M. Hein, T. Kaiser, and G. Müller, Phys. Rev. B **61**, 640 (2000).
[8] W. Kim, F. Marsiglio, and J. P. Carbotte, Phys. Rev. B **70**, 060505(R) (2004).
[9] J. I. Gittleman and B. Rosenblum, Phys. Rev. Lett. **16**, 734 (1966); J. Appl. Phys. **39**, 2617 (1968).
[10] M. W. Coffey and J. R. Clem, Phys. Rev. B **45**, 9872 (1992).
[11] C. J. van der Beek, V. B. Geshkenbein, and V. M. Vinokur, Phys. Rev. B **48**, 3393 (1993).
[12] E. B. Sonin and K. B. Traito, Phys. Rev. B **50**, 13547 (1994).
[13] Y. Enomoto and K. Okada, J. Phys.: Condens. Matter **9**, 10203 (1997).
[14] I. Aranson, B. Ya. Shapiro, and V. Vinokur, Phys. Rev. Lett. **76**,

142 (1996).
[15] G. W. Crabtree, D. O. Gunter, H. G. Kaper, A. E. Koshelev, G. K. Leaf, and V. M. Vinokur, Phys. Rev. B **61**, 1446 (2000).
[16] D. J. Priour, Jr. and H. A. Fertig, Phys. Rev. B **67**, 054504 (2003).
[17] D. Y. Vodolazov and F. M. Peeters, Phys. Rev. B **76**, 014521 (2007).
[18] A. B. Kolton, D. Dominguez, and N. Grønbech-Jensen, Phys. Rev. B **65**, 184508 (2002).
[19] A. Gurevich, Int. J. Mod. Phys. B **9**, 1045 (1995).
[20] E. H. Brandt, Rep. Prog. Phys. **58**, 1465 (1995).
[21] B. I. Ivlev, S. Mejia-Rosales, and M. N. Kunchur, Phys. Rev. B **60**, 12419 (1999).
[22] L. N. Bulaevskii and E. M. Chudnovsky, Phys. Rev. B **72**, 094518 (2005).
[23] A. I. Larkin and Yu. N. Ovchinnikov, Zh. Eksp. Teor. Fiz. **68**, 1915 (1975) [Sov. Phys. JETP **41**, 960 (1976)]; *Nonequilibrium Superconductivity*, edited by D. N. Langenberg and A. I. Larkin (North-Holland, Amsterdam 1986), p. 493.
[24] A. I. Bezuglyj and V. A. Shklovskij, Physica C **202**, 234 (1992).
[25] L. E. Musienko, I. M. Dmitrienko, and V. G. Volotskaya, Zh. Eksp. Teor. Fiz. **31**, 603 (1980) [JETP Lett. **31**, 567 (1980)].
[26] W. Klein, R. P. Huebener, S. Gauss, and J. Parisi, J. Low Temp. Phys. **61**, 413 (1985).
[27] S. G. Doettinger, R. P. Huebener, R. Gerdemann, A. Kühle, S. Anders, T. G. Träuble, and J. C. Villèger, Phys. Rev. Lett. **73**, 1691 (1994).
[28] A. V. Samoilov, M. Konczykowski, N.-C. Yeh, S. Berry, and C. C. Tsuei, Phys. Rev. Lett. **75**, 4118 (1995).
[29] Z. L. Xiao and P. Ziemann, Phys. Rev. B **53**, 15265 (1996).
[30] M. N. Kunchur, B. I. Ivlev, and J. M. Knight, Phys. Rev. Lett. **87**, 177001 (2001).
[31] B. Kalisky, P. Aronov, G. Koren, A. Shaulov, Y. Yeshurun, and R. P. Huebener, Phys. Rev. Lett. **97**, 067003 (2006).
[32] M. N. Kunchur, D. K. Christen, C. E. Klabunde, and J. M. Phillips, Phys. Rev. Lett. **72**, 752 (1994).
[33] M. N. Kunchur, J. Phys.: Condens. Matter **16**, R1183 (2004).
[34] A. V. Gurevich and R. G. Mints, Rev. Mod. Phys. **59**, 941 (1987).
[35] M. N. Kunchur, Phys. Rev. Lett. **89**, 137005 (2002).
[36] J. M. Knight and M. N. Kunchur, Phys. Rev. B **74**, 064512 (2006).
[37] C. P. Bean and J. D. Livingston, Phys. Rev. Lett. **12**, 14 (1964).
[38] L. Burlachkov, M. Konczykowski, Y. Yeshurun, and F. Hotzberg, J. Appl. Phys. **70**, 5759 (1991).
[39] F. Bass, V. D. Freilikher, B. Ya. Shapiro, and V. Shvaster, Physica C **260**, 231 (1996).
[40] A. Buzdin and M. Daumens, Physica C **294**, 257 (1998).
[41] D. Yu. Vodolazov, Phys. Rev. B **62**, 8691 (2000).
[42] E. H. Brandt, Phys. Rev. Lett. **69**, 1105 (1992).
[43] J. Matricon and D. Saint-James, Phys. Lett. **24A**, 241 (1967).
[44] L. Kramer, Phys. Rev. **170**, 475 (1968).
[45] H. J. Fink and A. G. Presson, Phys. Rev. **182**, 498 (1969).
[46] S. J. Chapman, SIAM J. Appl. Math. **55**, 1233 (1995).
[47] A. J. Dolgert, S. J. Di Bartolo, and A. T. Dorsey, Phys. Rev. B **53**, 5650 (1996).
[48] A. D. Hernandez and D. Dominguez, Phys. Rev. B **65**, 144529 (2002).
[49] G. D. Cody and R. L. Cohen, Rev. Mod. Phys. **36**, 121 (1964).
[50] L. Kramer and W. Pesch, Z. Phys. **269**, 59 (1974).
[51] J. Bardeen and R. D. Sherman, Phys. Rev. B **12**, 2634 (1975).
[52] A. I. Larkin and Yu. N. Ovchinnikov, Zh. Eksp. Teor. Fiz. **23**, 210 (1976) [JETP Lett. **23**, 187 (1976)].
[53] S. B. Kaplan, C. C. Chu, D. N. Landenberg, J. J. Chang, S. Jafarey, and D. J. Scalapino, Phys. Rev. B **14**, 4854 (1976).
[54] V. A. Shklovskii, Zh. Eksp. Teor. Fiz. **78**, 1281 (1980) [Sov. Phys. JETP **51**, 646 (1980)].
[55] F. C. Wellstood, C. Urbina, and J. Clarke, Phys. Rev. B **49**, 5942 (1994).
[56] J. R. Clem, Phys. Rev. Lett. **20**, 735 (1968).
[57] *Handbook of Mathematical Functions*, Natl. Bur. Stand. Appl. Math. Ser. No. 55, edited by M. Abramovitz and I. A. Stegun (U.S. GPO, Washington, D.C., 1964).
[58] H. Suhl, Phys. Rev. Lett. **14**, 226 (1965).
[59] A. van Ottrlo, M. Feigel'man, V. Geshkenbein, and G. Blatter, Phys. Rev. Lett. **75**, 3736 (1995).
[60] N. B. Kopnin and V. M. Vinokur, Phys. Rev. Lett. **81**, 3952 (1998).
[61] J.-M. Duan and E. Šimánek, Phys. Lett. A **190**, 118 (1994).
[62] M. W. Coffey, Phys. Rev. B **49**, 9774 (1994).
[63] E. M. Chudnovsky and A. B. Kuklov, Phys. Rev. Lett. **91**, 067004 (2003).
[64] I. Aranson, A. Gurevich, and V. Vinokur, Phys. Rev. Lett. **87**, 067003 (2001); I. S. Aranson, A. Gurevich, M. S. Welling, R. J. Wijngaarden, V. K. Vlasko-Vlasov, V. M. Vinokur, and U. Welp, *ibid.* **94**, 037002 (2005).
[65] E. Altshuler and T. H. Johansen, Rev. Mod. Phys. **76**, 471 (2004).
[66] P. Leiderer, J. Boneberg, P. Brull, V. Bujok, and S. Herminghaus, Phys. Rev. Lett. **71**, 2646 (1993); U. Bolz *et al.*, Europhys. Lett. **64**, 517 (2003); Physica C **388**, 715 (2003).
[67] C. A. Duran, P. Gammel, R. E. Miller, and D. J. Bishop, Phys. Rev. B **52**, 75 (1995).
[68] M. S. Welling *et al.*, Physica C **406**, 100 (2004).
[69] I. A. Rudnev *et al.*, Cryogenics **43**, 663 (2003).
[70] M. Baziljevich *et al.*, Physica C **369**, 93 (2002); T. H. Johansen *et al.*, Europhys. Lett. **59**, 599 (2002); F. L. Barkov, D. V. Shantsev, T. H. Johansen, P. E. Goa, W. N. Kang, H. J. Kim, E. M. Choi, and S. I. Lee, Phys. Rev. B **67**, 064513 (2003).
[71] B. Biechler, B-U. Runge, S. C. Wimbush, B. Holzapfel, and P. Leiderer, Supercond. Sci. Technol. **18**, 385 (2005).
[72] A. M. Campbell and J. E. Evetts, Adv. Phys. **21**, 199 (1972).
[73] R. P. Huebener, *Magnetic Flux Structures in Superconductors* (Springer-Verlag, Berlin, 1979).
[74] M. Rabinowitz, Appl. Phys. Lett. **16**, 419 (1970); J. Appl. Phys. **42**, 88 (1971).
[75] F. Palmer, Ph.D thesis, Cornell University, 1988 (unpublished).
[76] G. Ciovati, J. Appl. Phys. **96**, 1591 (2004).
[77] G. Ciovati, P. Kneisel, and A. Gurevich, Phys. Rev. ST Accel. Beams **10**, 062002 (2007).
[78] A. Granato and K. Lücke, J. Appl. Phys. **27**, 583 (1956).
[79] J. M. Pierce, J. Appl. Phys. **44**, 1342 (1973).
[80] B. Pioszyk, P. Kneisel, O. Stoltz, and J. Halbritter, IEEE Trans. Nucl. Sci. **20**, 108 (1973).
[81] K. Scharnberg, J. Appl. Phys. **48**, 3462 (1977).
[82] M. A. Hein, D. E. Oats, P. Hinst, R. G. Humphreys, and A. V. Velichko, Appl. Phys. Lett. **80**, 1007 (2002); M. A. Hein, R. G. Humphreys, P. Hinst, S. H. Park, and D. E. Oats, J. Supercond. **16**, 895 (2003).
[83] A. V. Velichko, M. J. Lancaster, and A. Porch, Supercond. Sci. Technol. **18**, R24 (2005).
[84] L. M. Fisher, A. V. Kalinov, I. F. Voloshin, I. V. Baltaga, A. V. Il'enko, and V. A. Yampol'skii, Solid State Commun. **97**, 833

(1996).
[85] M. Willemin, C. Rossel, J. Hofer, H. Keller, A. Erb, and E. Walker, Phys. Rev. B **58**, R5940 (1998).
[86] G. P. Mikitik and E. H. Brandt, Phys. Rev. B **67**, 104511 (2003); J. Low Temp. Phys. **139**, 221 (2005).
[87] R. H. Parmenter, RCA Rev. **23**, 323 (1962).
[88] J. Gittleman, B. Rosenblum, T. E. Seidel, and A. N. Wicklund, Phys. Rev. **137**, A527 (1965).
[89] M. P. Garfunkel, Phys. Rev. **173**, 516 (1968).
[90] T. Dahm and D. J. Scalapino, Phys. Rev. B **60**, 13125 (1999).
[91] A. Gurevich, Physica C **441**, 381 (2006).
[92] J. Halbritter, J. Supercond. **8**, 691 (1995).
[93] A. Gurevich, Phys. Rev. B **65**, 214531 (2002).
[94] Ya. B. Zel'dovich, G. I. Barenblatt, V. B. Librovich, and G. M. Makhviladze, *The Mathematical Theory of Combustion and Explosion* (Consultans Bureau, New York, 1985).
[95] P. Bauer, N. Solyak, G. Ciovati, G. Eremeev, A. Gurevich, L. Lilje, and B. Visentin, Physica C **441**, 51 (2006).
[96] G. Ciovati, Appl. Phys. Lett. **89**, 022507 (2006).
[97] A. Gurevich, Appl. Phys. Lett. **88**, 012511 (2006).
[98] S. M. Deambrosis, G. Keppel, V. Ramazzo, C. Roncolato, R. G. Sharmy, and V. Palmieri, Physica C **441**, 108 (2006).
[99] E. W. Collings, M. D. Sumption, and T. Tajima, Supercond. Sci. Technol. **17**, S595 (2004).
[100] B. Jin, P. Kuzel, F. Kadlec, T. Dahm, J. M. Redwing, A. V. Pogrebnyakov, X. X. Xi, and N. Klein, Appl. Phys. Lett. **87**, 092503 (2005).